AD_____

Award Number: DAMD17-98-1-8511

TITLE: A Novel High Resolution Positron Emission Tomography
System for Measurement of Bone Metabolism

PRINCIPAL INVESTIGATOR: John A. Correia, Ph.D.

CONTRACTING ORGANIZATION: Massachusetts General Hospital
                           Boston, Massachusetts 02114

REPORT DATE: September 2001

TYPE OF REPORT: Annual

PREPARED FOR: U.S. Army Medical Research and Materiel Command
               Fort Detrick, Maryland 21702-5012

DISTRIBUTION STATEMENT: Approved for Public Release;
                        Distribution Unlimited

The views, opinions and/or findings contained in this report are
those of the author(s) and should not be construed as an official
Department of the Army position, policy or decision unless so
designated by other documentation.

REPORT DOCUMENTATION PAGE

Public reporting burden for this collection of information is estimated to average 1 hour per response, including the time for reviewing instructions, searching existing data sources, gathering and maintaining the data needed, and completing and reviewing this collection of information. Send comments regarding this burden estimate or any other aspect of this collection of information, including suggestions for reducing this burden to Washington Headquarters Services, Directorate for Information Operations and Reports, 1215 Jefferson Davis Highway, Suite 1204, Arlington, VA 22202-4302, and to the Office of Management and Budget, Paperwork Reduction Project (0704-0188), Washington, DC 20503

1. AGENCY USE ONLY (Leave blank)	2. REPORT DATE September 2001	3. REPORT TYPE AND DATES COVERED Annual (1 Sep 00 - 31 Aug 01)

4. TITLE AND SUBTITLE A Novel High Resolution Positron Emission Tomography System for Measurement of Bone Metabolism	5. FUNDING NUMBERS DAMD17-98-1-8511

6. AUTHOR(S)
John A. Correia, Ph.D.

7. PERFORMING ORGANIZATION NAME(S) AND ADDRESS(ES) Massachusetts General Hospital Boston, Massachusetts 02114 E-Mail: correia@pet.mgh.harvard.edu	8. PERFORMING ORGANIZATION REPORT NUMBER

9. SPONSORING / MONITORING AGENCY NAME(S) AND ADDRESS(ES) U.S. Army Medical Research and Materiel Command Fort Detrick, Maryland 21702-5012	10. SPONSORING / MONITORING AGENCY REPORT NUMBER

11. SUPPLEMENTARY NOTES

12a. DISTRIBUTION / AVAILABILITY STATEMENT Approved for Public Release; Distribution Unlimited	12b. DISTRIBUTION CODE

13. ABSTRACT (Maximum 200 Words)

The purpose of the work reported here is to develop high-resolution PET instrumentation for imaging the long bones. To-date a single plane prototype and a single plane second-generation instrumentation have been completed. The latter is currently being evaluated. A generalized multi-planar detector element has also been designed and evaluated experimentally and a volumetric instrument has been designed through simulation studies. A radiopharmaceutical for bone growth rate imaging, labeled tetracycline is currently being developed for use in a demonstration study of imaging in a monkey osteoporosis model.

14. SUBJECT TERMS	15. NUMBER OF PAGES 40
	16. PRICE CODE

17. SECURITY CLASSIFICATION OF REPORT Unclassified	18. SECURITY CLASSIFICATION OF THIS PAGE Unclassified	19. SECURITY CLASSIFICATION OF ABSTRACT Unclassified	20. LIMITATION OF ABSTRACT Unlimited

NSN 7540-01-280-5500

Standard Form 298 (Rev. 2-89)
Prescribed by ANSI Std. Z39-18
298-102

Table of Contents

II. Report Body:

A. Introduction:

The overall aims of this project are:

1. To design and develop an instrument for high resolution PET imaging in long bones.
2. To demonstrate the use of this instrument in an experimental protocol involving the assessment of estrogen therapy for osteoporosis in a monkey model.

During the current project period we have completed construction of the second, final single –plane instrument, explored methods of improving its performance, developed a design for a generalized volumetric version of the instrument and pursued the radiochemical synthesis of 11-C and 18-F tetracycline. We are currently behind schedule in beginning studies in monkeys due to difficulties with the chemical syntheses. To help address these difficulties we have temporarily increased the amount of chemist effort (as of July 1, 2001) from 10% to approximately 70% by adding 50% of a laboratory chemist (Dr. Choi) and retaining the consulting services (at no charge to the project) of a senior radiochemist (Dr. Elmaleh) and a senior biochemist (Dr. Carter) at our institution. With the addition of these individuals we have begun to make better progress and expect to solve the outstanding problems within the next two months.

The single plane instrument has been used in a large number of small-animal studies funded under a related DOD project at our institution (DAMD-17-99-1-9555, Dr. A. Brownell, principal investigator).

B. Design studies for a Volumetric PET Instrument:

In the last project period we reported some preliminary studies of a volumetric detector element design which is a generalization of our single plane detector element. During the current project period we have extended these studies and have evolved a preliminary design for a volumetric instrument. Figure 1 shows the detector block design. The LSO crystals are discrete in the radial direction (i.e., in-plane) and continuous in the axial (or z) dimension. Our initial studies with 1.2x5x15mm crystals, reported previously, showed that this approach is feasible. We have evaluated crystals of various dimensions more thoroughly during the present period in an attempt to extend the axial dimension of the block.
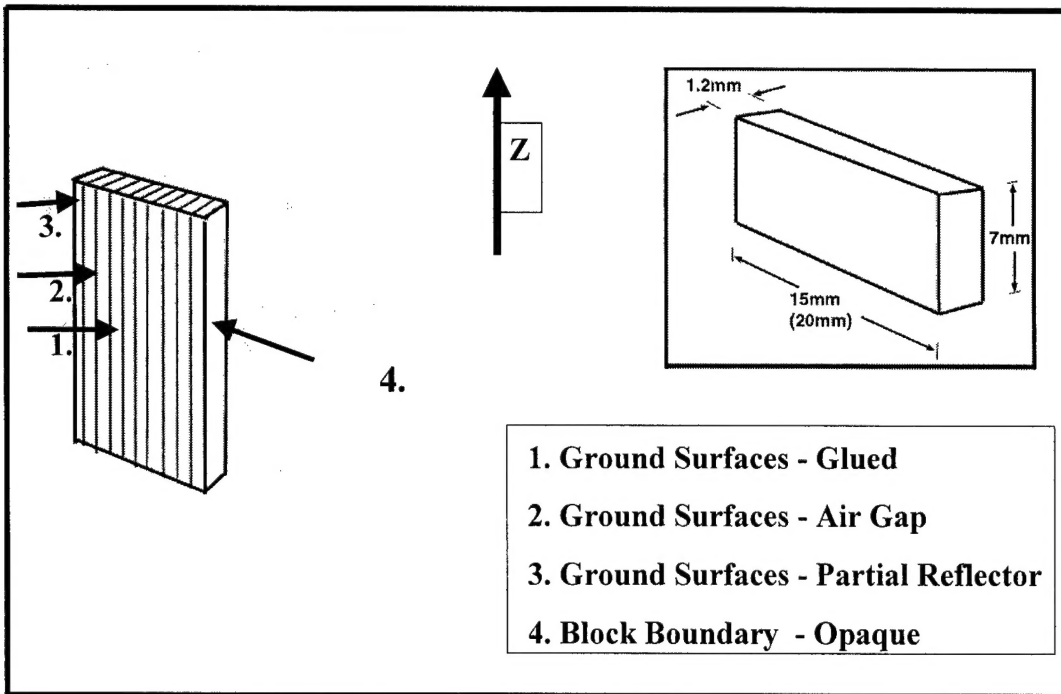
4

Figure 1: Volumetric LSO block design showing block, phototubes, individual crystal dimensions and crystal interface preparations.

The surface preparations are similar to those of the 10 and 12-crystal 1-dimensional blocks reported previously. The faces of the middle six crystals are glued together, the next one on either side is separated by an air gap and the outer two are separated by a partially translucent Teflon barrier. The basis of this design is that light collected and used to identify a given crystal within the block also contains information on the vertical (z) position of the interaction within the block. Thus, if the z thickness of the crystals is extended, it is possible not only to identify which crystal gave rise to the interaction but also, by a separate computation using the same PMT signals, to obtain the z-coordinate of the interaction.

. Measurements were made after adjusting the gains of the PMT's to give the same signal response to a uniform field. The uniform field source of 511 keV was then used to irradiate the block at several different z-positions with respect to the block- center. The radial ratio was calculated for a 10:1 range of whole-block signal response as follows:

RADIAL RATIO = $[(A+C)-(B+D)]/[(A+C)+(B+D)]$.

Where A, B, C and D are the respective outputs of the four phototubes. The radial ratio data were binned into narrow bins (approximately 2 mm) based on the axial ratio (see below). Figure 2 shows typical results for the 1.2 x 7 x 20mm, 10 crystal block. Note that the 10 crystals are well resolved out to +/- 8 mm from the block center.
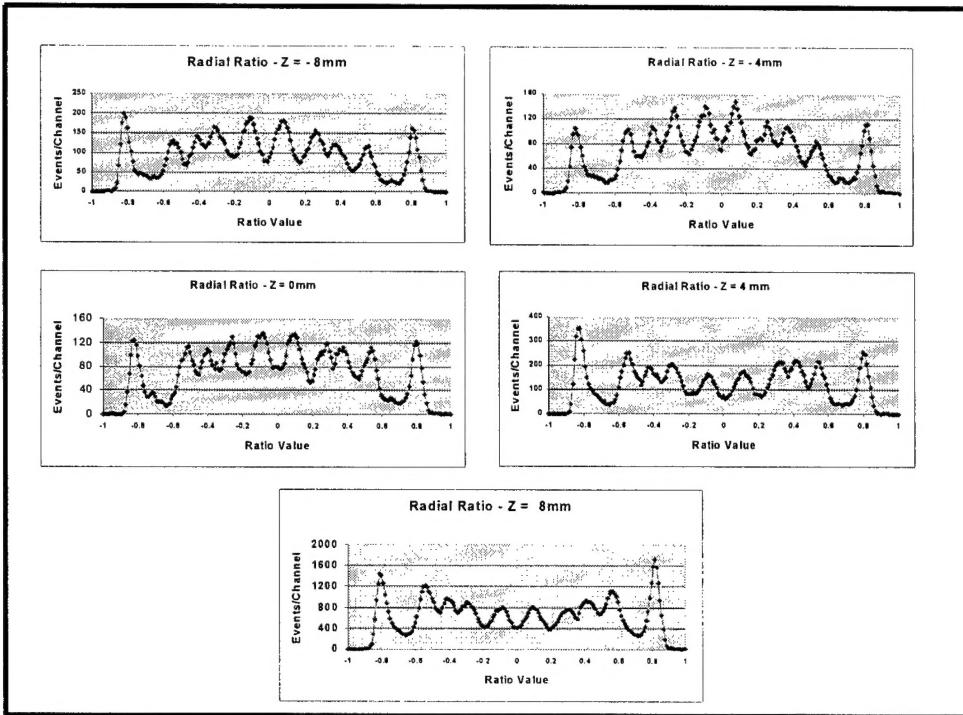
Figure 2: Examples of the 2D block radial ratio for different z-positions of a uniform field of 18-F source computed from PMT signals as indicated in the text. The ten crystals are well identified out to +/- 8mm from the block center.

To assess axial performance, the z-axis ratio was measured for a 10:1 signal range using a collimated line source. Measurements were made with the source positioned at the block center and at z positions up to 8mm from center in 1.6mm steps. The z-axis ratios computed as follows:

Z-RATIO=[(A+B)-(C+D)]/[(A+B)+(C+D)].

Where A, B, C, and D are the phototube outputs. The responses are well separated over the central region of the block and there is still reasonable separation out to about +/- 8 mm. Typical results are shown in figure 3. These measurements are for single photon events and it should be kept in mind that the coincidence resolution in a PET system will be better than that shown here by a factor of 0.7.

Based on experiments with the various blocks a preliminary design for a volumetric PET system has been generated. The sensitivity improvement for such a system compared to the single ring systems has been studied by Monte Carlo simulation for the two best block geometries. Each has 10 crystals with respective dimensions 1.2x5x15mm and 1.2x7x20mm. The computed sensitivities for both extended cylindrical sources and point sources are shown in figure 4. The best expected improvement in sensitivity will be approximately a factor of 20 for extended sources and a factor of four for point objects. The scatter fraction was also simulated for the open volumetric geometry and

extended objects. The results, shown in figure 5, indicate that scatter the scatter fraction will be below 10% for activity filled objects which encompasses almost the entire field. Figure 6 lists the specifications of an instrument based on these detector elements and a sketch of its geometry.
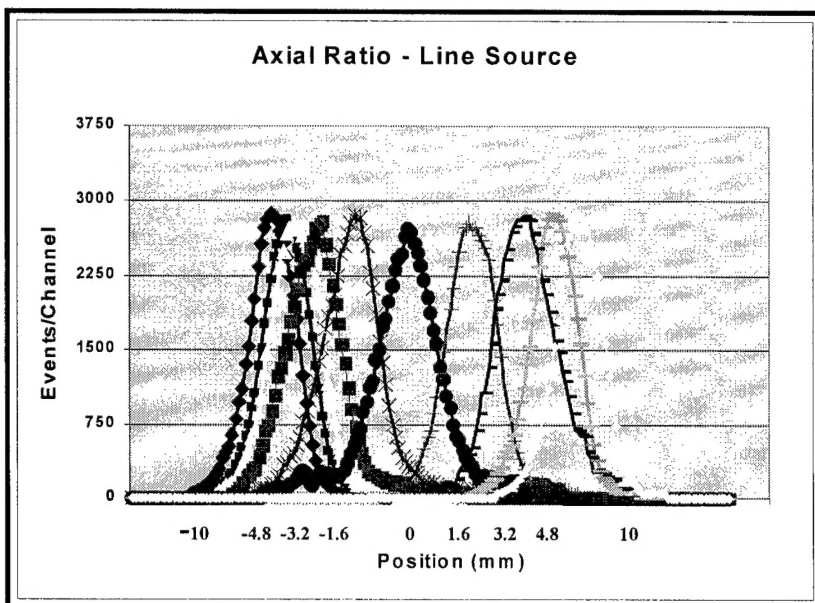

Figure 3: Z-ratio measurements in a block of 1.2x7x20mm crystals. The source positions in 1.6mm increments are well resolved at the center. At distances up to 8mm from the block center the resolution is poorer but the z-ratio still maintains some sensitivity to change. Note that the nonlinear x scale reflects the changing response of the detector with position.
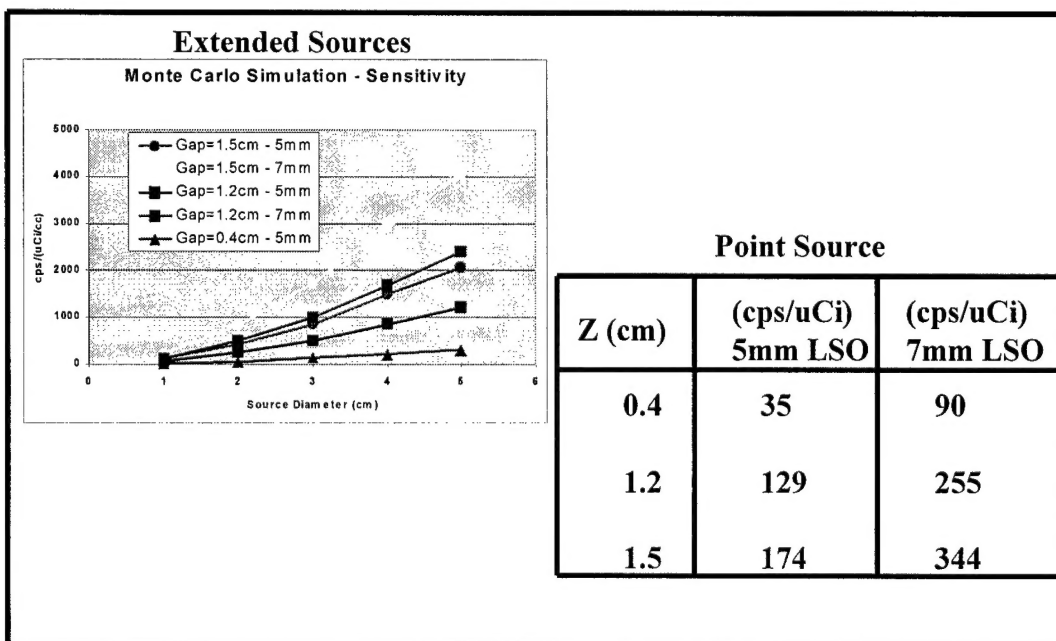

| Point Source | | |
Z (cm)	(cps/uCi) 5mm LSO	(cps/uCi) 7mm LSO
0.4	35	90
1.2	129	255
1.5	174	344

Figure 4: Monte Carlo simulated sensitivity for volumetric designs for point and cylindrical objects.

Scatter Fraction - 2D Detector

Figure 5: Monte Carlo simulation f volumetric PET scatter fraction.

VOLUMETRIC INSTRUMENT

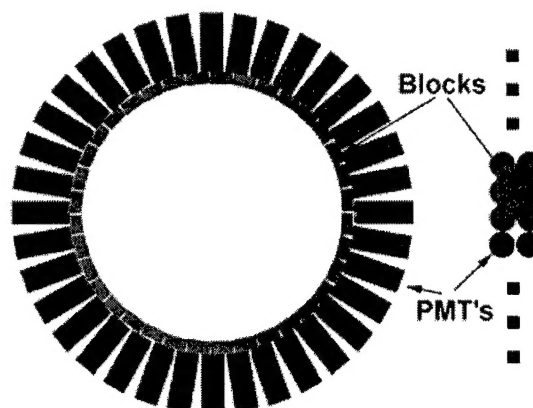| PARAMETER	VALUE
DIAMETER	14.7cm
CRYSTALS	360: 1.2 x 15 x 7mm
RESOLUTION	
Center	1.2mm
2.5cm Radius	1.7mm
Axial	1.3-1.6mm
PT. SRC. SENS.	350 cps/uCi

Figure 6: Specifications and sketch of volumetric design.

The volumetric design will use a straightforward generalization the electronics and acquisition system used in the single plane devices. An important aspect of the detector design is that it is relatively inexpensive and easily fabricated.

8

C. Progress in Radiolabeling of Tetracycline:

Labeling with Iodine:

124-I is a potentially useful radioisotope for PET imaging. It is however not readily available commercially at this time. We have been attempting to bring 124-I production on-line at our cyclotron facility under other funding but not established routine production as yet. Anticipating the availability of 124-I we have carried out labeling and biodistribution studies with 125-I, a longer-lived, readily available non-PET isotope of Iodine.

Tetracycline has been labeled with 125-I through exchange labeling using labeled NaI. Its biodistribution was measured in eight control rats and eight rats that had been subjected to a burn model for under another approved project in our laboratory. Rats were co-injected with 125-I tetracycline and 99m-Tc MDP, a bone imaging agent. The animals were sacrificed one hour post injection and dissected. Average organ and structure radioactivity concentrations were subsequently determined by well counting. Also, similar data using 18F-fluoride ion was obtained. The results of these studies are summarized in figure 7.The levels of tetracycline in bone appear adequate for imaging at this early post injection time. Although they lower than either 99m-Tc or 18F-fluoride ion, it should be noted that tetracycline is tracing a much smaller distribution volume, that of newly forming bone.

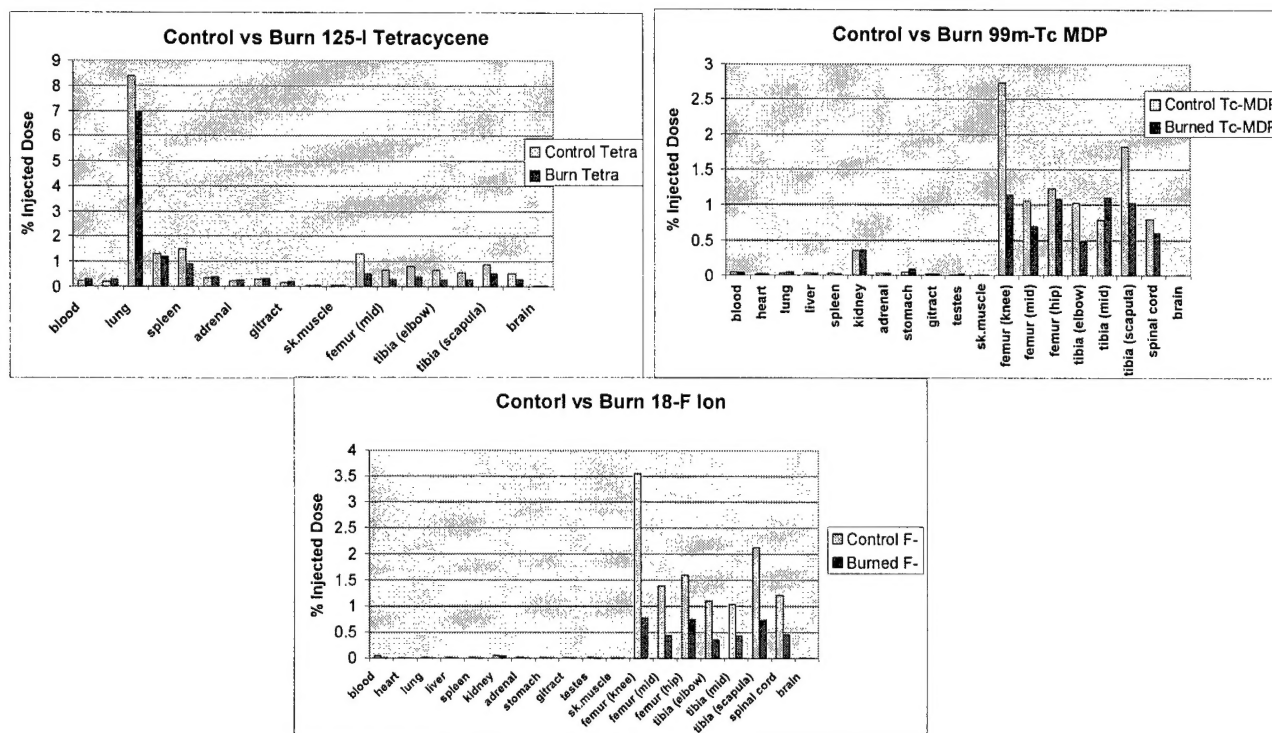Figure 7: Average organ concentrations at 1 hour post-injection of 125-I tetracycline, 99m-Tc MDP and 18-F fluoride ion in normal and burned rats.

11-C and 18-F Exchange Labeling:

A series of experiments were carried out to determine if tetracycline could be labeled with 18-F by pre-labeling with non-radioactive iodine and then exchanging for 18-F. This method did not work well and resulted in very low yields.

Current Efforts:

Several more complex labeling approaches are currently being tested in the laboratory. They attempt to address two problems. The first is the low solubility of commonly available tetracyclines in organic solvents and the second is the likely need to protect the phenol-OH and keto groups on the molecule during labeling.

Tetracycline hydrate   N-demethylated Tetracycline HC
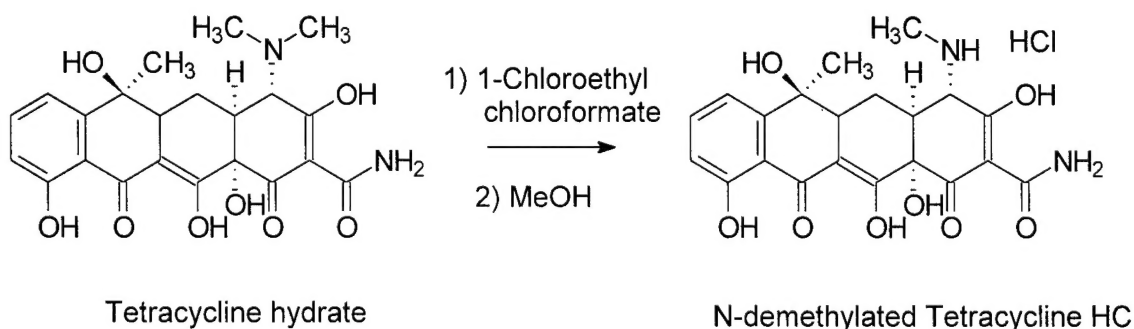
Figure 8

The scheme of figure 8 illustrates the de-methylation of tetracycline. The hydrate form has low solubility in common organic solvents. Experiments with a standard methylation reaction using CH_3I, DMF and K_2CO_3 resulted in very low conversion. Such conversion may improve with the imposition of extreme conditions such as high, temperature, excess base, or excess alkylating agent. To better evaluate the variants in to this approach we are in the process of setting up a reverse phase TLC system. Also we are evaluation the use of other solvents such as DMSO.

We have also begun studies of how to protect the phenolic, OH and/or keytone groups with a Bz or 1,3-dioxolane group. This should improve the stability of the product and also improve solubility in organic solvents. Dehydration of the hydrate form of tetracycline may improve the reaction by increasing solubility. Several standard de-protection. A more complete reaction scheme is illustrated in figure 9. The steps are as follows:

1. Protection of phenolic-OH.
2. Protection of ketone.
3. De-methylation of protected tetracycline.
4. 11-C Radiolabeling.

3. . Deprotection.
4. . HPLC separation of product.

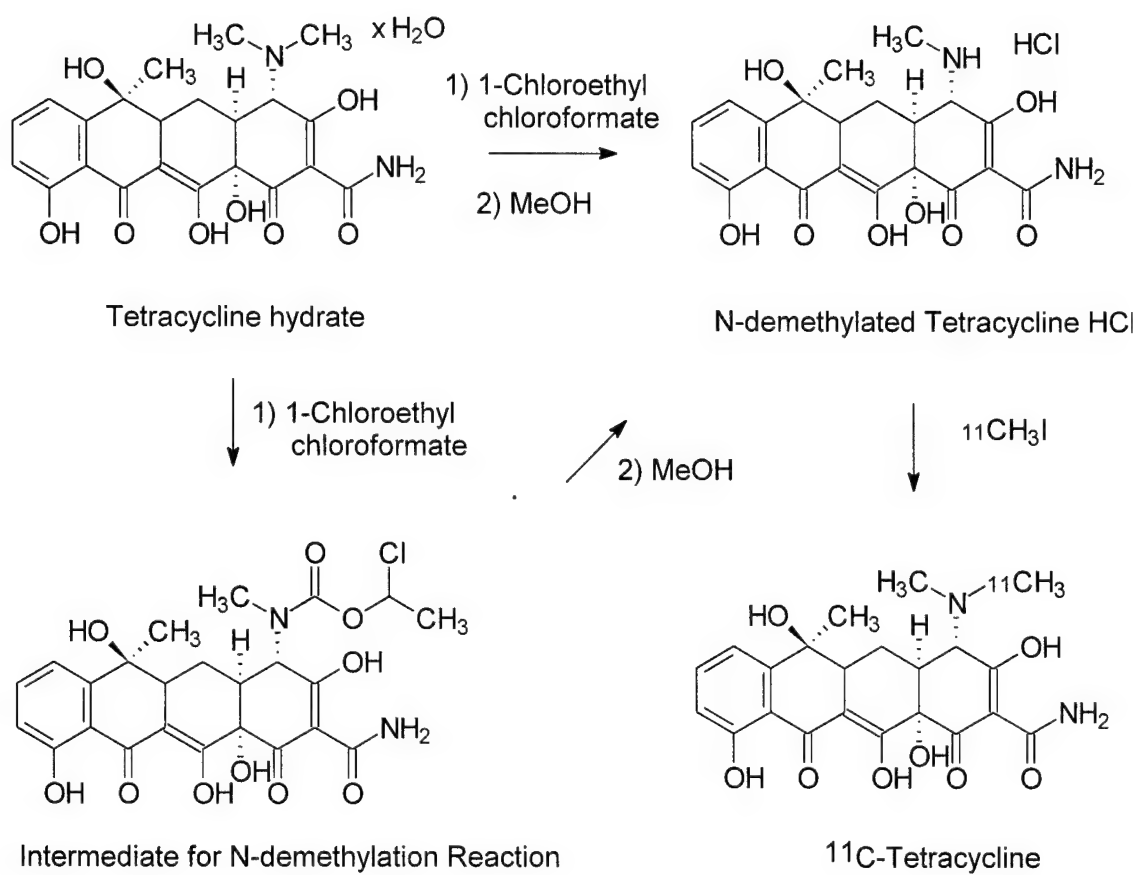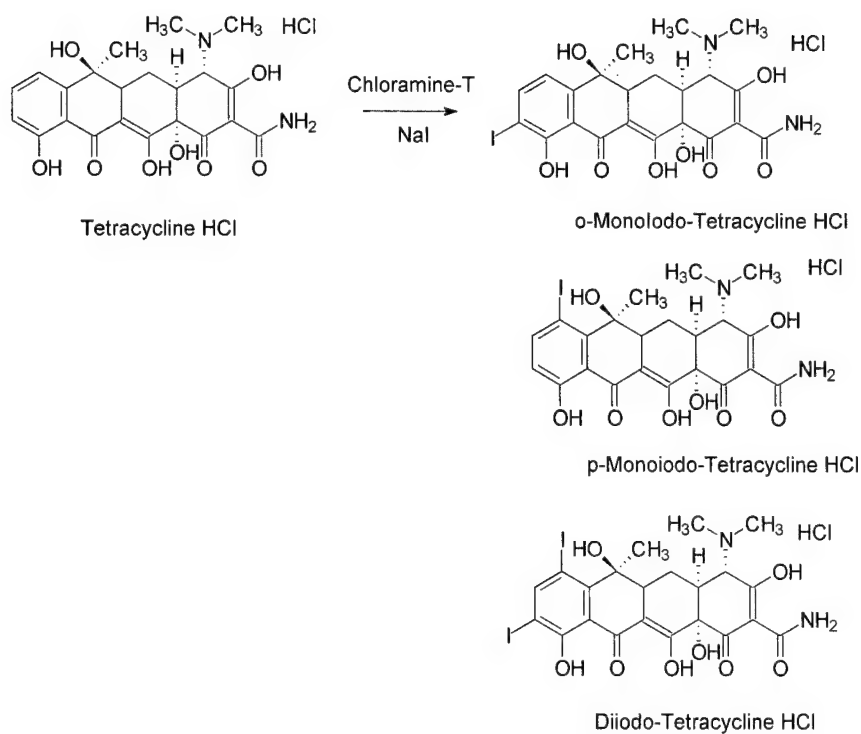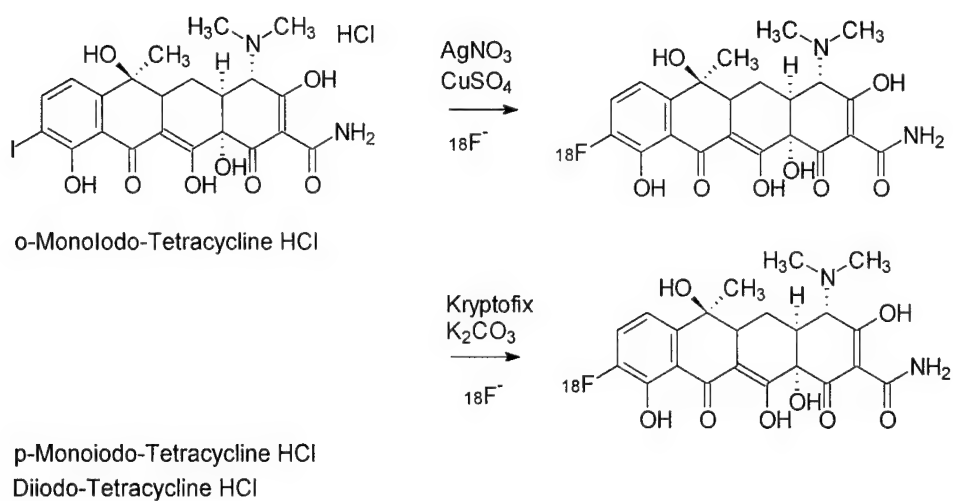Steps 1-3 have been completed to-date.

Figure 9.

Figure 10.

Figure 11.

Figures 10 and 11 illustrate an iodination approach, eventually leading to 18-F labeling, which is also under development. This approach has been used successfully with other compounds in our laboratory.

In order to address the problem of producing a useable PET labeled tetracycline, the absence of which is holding up the animal imaging phase of the project, we have recently intensified our efforts. We have temporarily added a 50% chemist. Dr. Choi, to the group as well as a two senior consultants, Dr. Elmaleh a senior radiochemist and Dr. Carter, a senior biochemist at no charge to the project). We have already made some progress and expect results for both 11-C and 18-F labeling within the next two months.

D. Single-Plane Instrument Status and Improvements:

The prototype single plane instrument completed in year 1 of the project is in routine use (see below). The final instrument is essentially completed and is undergoing testing and calibration. The properties of these instruments are summarized in table 1.

In order to improve the light output of the LSO crystals, chemical etching was explored. Several workers in the field have demonstrated improved light output in polished crystals upon chemical etching of the surfaces. The crystals in our single plane instruments have ground, rather than polished surfaces but it was postulated that mild etching might improve light yield. Test crystals were placed in a concentrated phosphoric acid bath at 130 degrees centigrade for various times from 0.5 to 10 minutes and then washed with 1N HCL and distilled

	GENERATION-1	GENERATION-2
DIAMETER	12.3cm	14.7cm
CRYSTALS	360: 1x4.5x5mm	360: 1.2x4.5x7mm
RESOLUTION **Center** **2.5cm Radius**	1.16mm 1.60mm	1.2mm 1.7mm
PT SRC SENS	35 cps/uCi	105 cps/uCi

Table 1: Summary of Single-Plane Instruments Constructed.

water. The crystals were suspended by Teflon holders so that all surfaces would be equally exposed to the acid. The best results in terms of light output were achieved at about 5 minutes

etching. Typical improvements in light output of about 10% were observed at 10 minutes etching. The average change in volume of the crystals subjected to etching is minimal. A sample of 25 crystals subjected to 10 minute etching had average volume loss of 2%. Figure 11 illustrates typical energy spectra from an etched and an unetched crystal. Two spectra are shown for each crystal. One with the crystal placed mounted its side to a phototube behind a Teflon reflector. This geometry will result in 100% light collection. The second spectrum is taken with the crystal mounted to the phototube at one of its small faces (ends). The improvement in light output is defined as the difference in the rations of the two photopeak locations for each crystal.
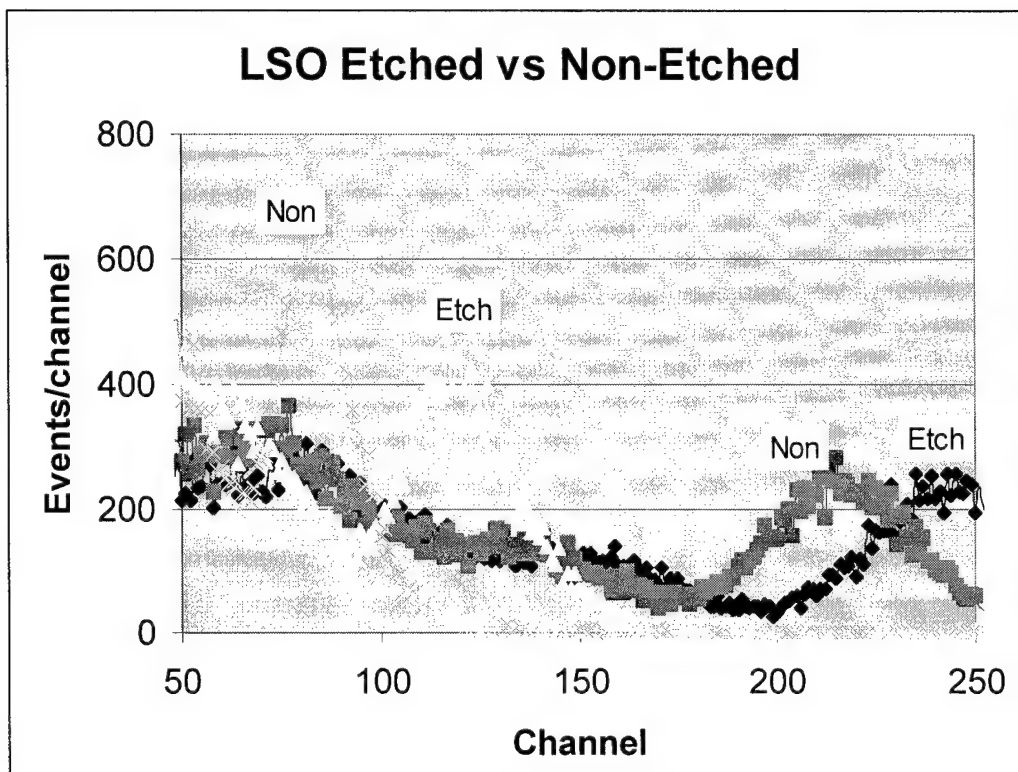

Figure 11: Energy spectra of etched vs. non-etched LSO crystals. The lower spectra (photopeaks at approximately channel 75) are from the crystal ends and the higher spectra are from the crystal sides with a Teflon reflector to collect all light.

In order to the increase the high countrate performance of the single plane instruments we have developed a new hardware interface which uses the PCI bus as its final point of entry into the computer. This interface has been designed, tested and implemented on the single plane system. It is built around a commercially purchased buffering and transfer card (PCDIO3240, Cyber Systems). The quantity of data transferred at high rates (20,000 events per second) is on the order of 700,000 transfers per second, which must be synchronized in groups of 36 (or 30 in the case of the prototype) phototube signals representing each event. With the old interface the systems were limited

to about 5,000 events (or 150,000-180,00 transfers) per second by bus deadtime and software overhead. The new approach provides start and stop pulses to the PCDIO buffer card to maintain synchronization and clocking pulses to transfer each event. The buffer in the PCDIO card is then periodically read into the computer under software control. A schematic of the interface is shown in figure 12.
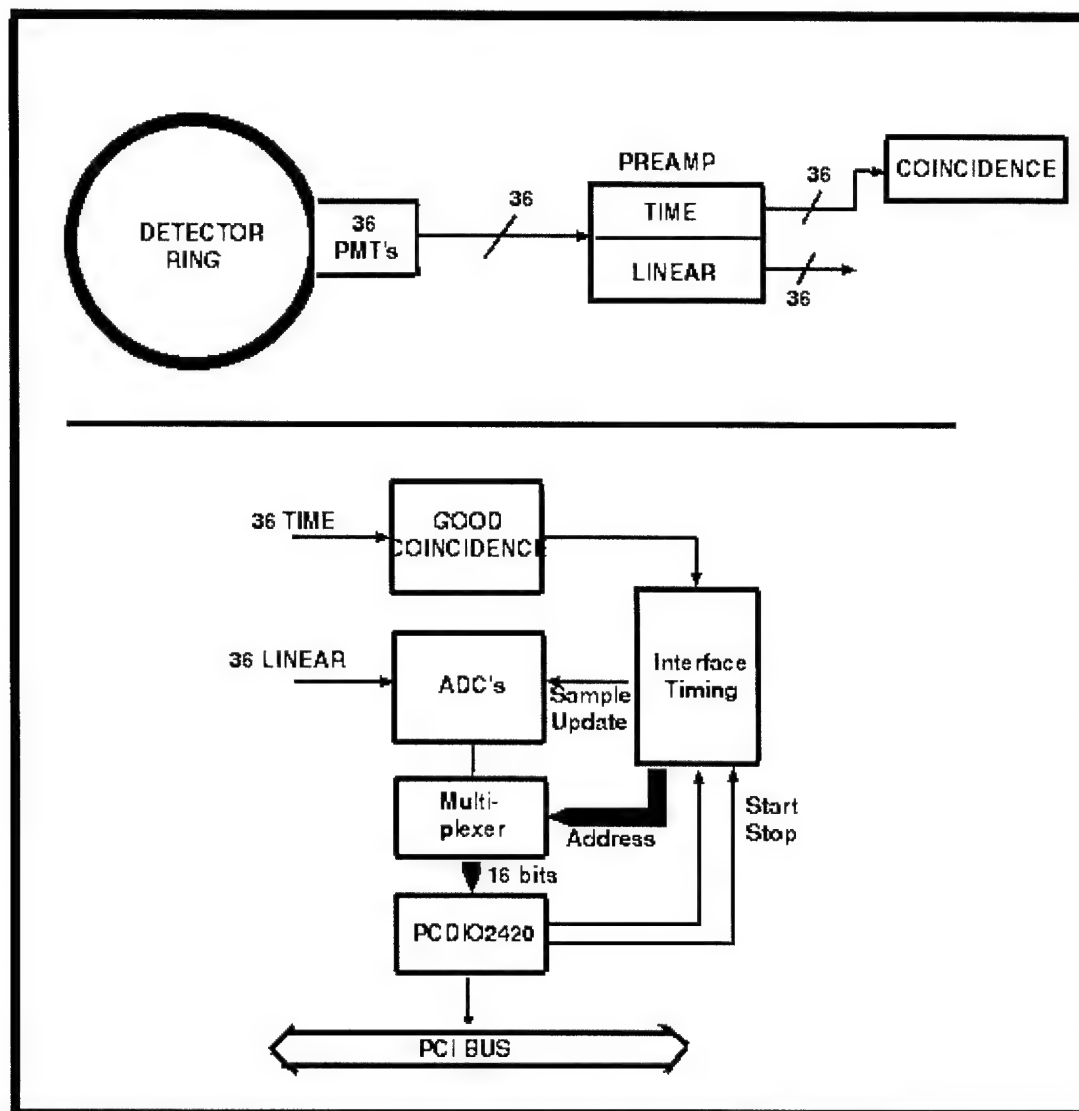

Figure 12: Upper: schematic of data output from camera. Lower: schematic of high data rate interface.

E. Animal Studies Carried out by Related DOE Projects Using Instruments:

A DOD-funded project at our institution which is closely related this one is DAMD17-99-1-9555 entitled "Evaluation of Early and Prolonged Effects of Neurotoxicity using Functional Imaging Techniques" (A.L. Brownell, P.I.) Studies of small animals under this program using the instrumentation developed by our effort are part of this program. During the last year Dr. Brownell and her co-workers have carried out the following studies using our single plane instruments:

1. Thirty-five 18-F-Fluorodeoxyglucose brain studies in rats.
2. Thirty-six 18-F-Fluorodeoxyglucose brain studies in mice.
3. Eight 11C neuoro-receptor studies in rats.

Two examples of these studies are shown in figures 13 and 14.

Fused PET (18F-FDG accumulation) and T2 weighted MR images after acute 3NP neurotoxicity in rat brain

7.4mm   7.5mm   7.6mm   7.7mm   7.8mm   8.0mm
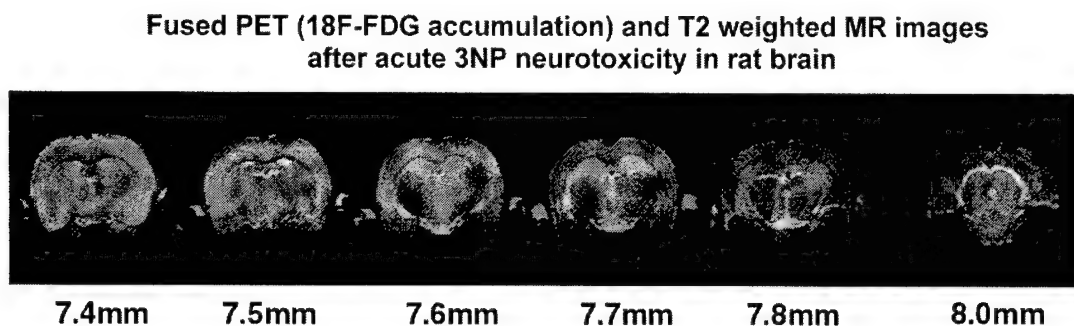
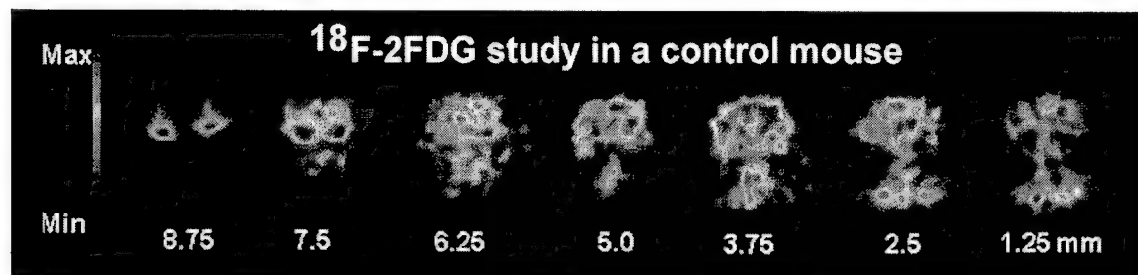Figure 13: Example of PET study in rat brain registered with MRI.

Figure 14: Example of normal mouse brain coronal FDG Images.

VI. Key Research Accomplishments:

1. Completion of single plane PET instruments.

2. Studies to improve detector element performance and high countrate performance of single plane instruments.

3. Completion of a design for a volumetric generalization of the single plane instruments.

4. Determination of synthesis schemes for labeling of tetracycline.

VII. Reportable Outcomes:

1. Construction of single-plane 1mm resolution PET instruments. Published, patent being pursued through MGH.

2. Completion of Volumetric block design. Partially published. Patent on detector module design being pursued.

3. Design of Volumetric PET instrument. In Press. Patent on Instument being pursued.

VIII. Conclusions:

During the first year of the project we established the design of a high resolution PET instrument for bone imaging and constructed a prototype. During the second year we physically characterized the prototype, modified our design and began construction of a final single plane device. The construction of this device was completed in the current year. Beginning in the second year and continuing through the current year we developed a generalized detector element and a system design for multi-planar (or volumetric) imaging. During year 2 and the current year we have worked on the development of labeled tetracycline for bone imaging. We have successfully labeled it with iodine and carried out biodistribution studies in rats. A number of approaches to 11-C and 18F labeling were explored without success. Since this compound is essential to the animal study phase of the project, we have made a major increase in the labeling effort and have had some success in producing precursors. We expect

that, with the increased effort, we will be successful within the next few months allowing us to move on to animal imaging.

VI. Appendix.

Previously Reported:

1. "Development of a Small Animal Pet Imaging Device with Resolution Approaching 1mm", JA Correia, CA Burnham, D Kaufman, AJ Fischman, J Nucl Med 40:285P (1999) Abstr.

2. "Development of a Small Animal Pet Imaging Device with Resolution Approaching 1mm", JA Correia, CA Burnham, D Kaufman, AJ Fischman, IEEE Trans Nucl Sci 46:631-635 (1999).

3. "A Pet Imaging Instrument for High Resolution Rat and Mouse Imaging ", JA Correia, CA Burnham, D Kaufman, E. Carter, AL Brownell, AJ Fischman, "High Resolution Imaging in Small Animals with PET, MRI and other Modalities: Proceedings", pp 63-64, Amsterdam (1999).

4. "Performance of a Small Animal Pet Imaging Device with Resolution Approaching 1mm", JA Correia, CA Burnham, D Kaufman, AJ Fischman, IEEE Nuclear Science Symposium and Medical Imaging Conference Record, M7:pp 1-5 (1999).

5. "Designs for Small Animal PET Systems" ,Abstr., JA Correia, CA Burnham, D Kaufman, AJ Fischman, Congress of European Assoc. Nuclear Med, (Sept, 2000).

New Since Last Report:

6. Design Considerations for Small-Animal PET Devices with Resolution Approaching 1 mm", JA Correia, CA Burnham, D Kaufman, AJ Fischman, , IEEE Nuclear Science Symposium and Medical Imaging Conference Record,pp 21:41-45 (2001).

7. " Design of a Volumetric High Resolution Small Animal PET ", JA Correia, CA Burnham, D Kaufman, AJ Fischman, "High Resolution Imaging in Small Animals: Proceedings", pp 187-188, (2001).

8. " An LSO-based detector element for a Multiplanar small animal PET instrument", JA Correia, CA Burnham, D Kaufman, AJ Fischman, J Nucl Med 41:56P (2001) Abstr.

Development of a Small Animal PET Imaging Device with Resolution Approaching 1mm

J.A. Correia, C.A. Burnham, *Senior Member IEEE*, D. Kaufman, A.J. Fischman

Massachusetts General Hospital, and Harvard Medical School, Boston, MA 02114

Abstract

The work presented here describes progress in the design and construction of a single-plane PET tomograph having spatial resolution approaching 1 mm. The system consists of a 12 cm diameter ring with 360 LSO detectors viewed by 30 photo-multiplier tubes. Thin (5 mm) crystals and a low energy threshold are used. Crystals are identified using both position arithmetic and energy criteria. To-date the system construction has been completed, system tuning carried out and imaging studies begun.

I. INTRODUCTION

Positron emission tomography (PET) has achieved major successes during the past ten years as a metabolic imaging modality, especially in human and large animal subjects. Instrumentation for use in these regimes has become highly developed and reliable and is used routinely in many laboratories throughout the world. Recently, a number of workers have designed and successfully constructed instruments which image at higher resolution over small-scale fields, with the goal of imaging small animals such as monkeys, rats and mice [1-11].

Small animal imaging presents a situation where positron range effects and sampling are the dominant physical limitations. Annihilation-pair non-co-linearity and photon scatter are minimized due to the small dimensions of both instrument and subject. Theoretical and simulation studies support the idea that spatial resolution on the order of 1mm can be achieved with ^{18}F and ^{11}C [12-14]. The availability of LSO as a scintillator material for PET leads to several possible approaches to designing detector modules for PET systems having spatial resolution approaching one millimeter [15].

The purpose of the work reported here was to assess the feasibility of 1mm imaging by designing and constructing a prototype high resolution PET instrument using LSO detectors. The approach taken was to design and construct a simple prototype with as much flexibility as possible in hardware and software implementation. A simple design allows for straightforward modification and adaptation.

II. SYSTEM DESIGN

A. General Design

Simulation studies of the geometry including positron range, annihilation non-co-linearity and scatter have been used to develop the design presented here. The approach maximizes the use of software data processing to minimize electronics construction and maintain flexibility. A system block diagram is shown in figure 1.
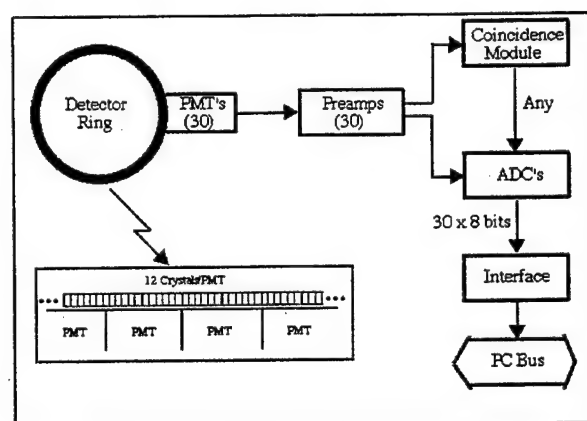

Figure 1: System Block Diagram

The detector array consists of a single ring of 360 1x4.5x5 mm LSO crystals organized into blocks of 12 crystals each viewed by two RCA 647 photomultipliers (PMT's) in a one dimensional implementation of the geometry proposed by Wong [16]. To achieve high resolution, thin crystals (0.5 cm) are used for several reasons; first, the use of thin crystals moderates the degradation and non-uniformity of resolution caused by multiple detector penetration at photon incidence angles far from the normal, and secondly, blurring due to multiple interaction sites is reduced [14]. The choice of thin crystals represents a sacrifice in sensitivity to preserve resolution.

The PM Tube signals are processed for timing and position. The coincidence logic uses the timing signal to identify any coincidence event from the central volume of the detector. The coincidence resolving time of the circuitry is 16 ns. The 30 linear position signals are DC coupled to the sample-and-hold ADC. Pulse shaping equivalent to single

$$R = (A - kB) / (A + kB) \qquad (1)$$

and if an energy criterion to select only photopeak events:

$$E > E_{threshold} \quad \text{and} \quad E_{lower} < E < E_{upper} \qquad (2)$$

is met, a particular crystal is identified, otherwise the event is rejected.

A plot of the **R** spectrum from a typical block is shown in figure 4. Figure 5 shows the average bounds for the 30 blocks and figure 6 the individual-crystal energy spectra from a typical block.
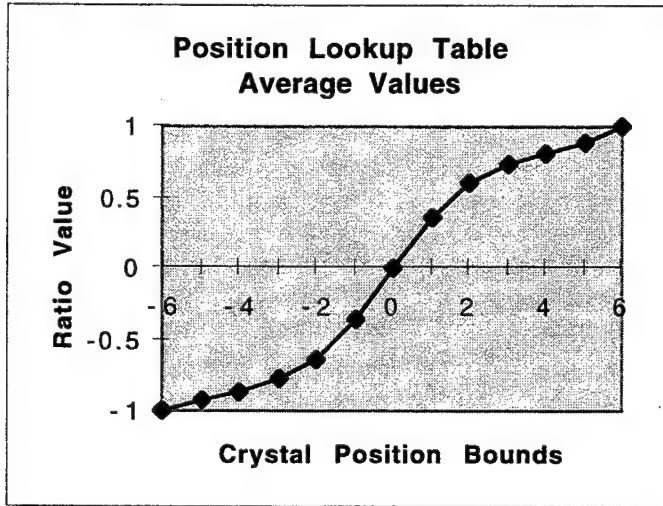

Position Lookup Table Average Values

Figure 5: Measured ratios averaged over 30 blocks plotted as a function of ratio with crystal bounds indicated.

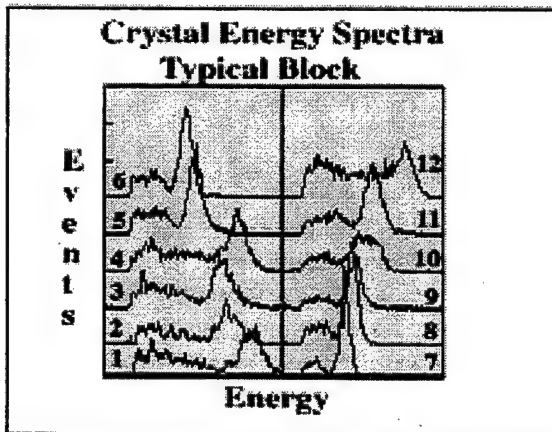**Crystal Energy Spectra Typical Block**

Figure 6: Energy spectra measured from a typical block using a ^{68}Ge source.

The PMT gains are adjusted such that the maximum signal of each utilizes the full dynamic range of the ADC. A

gain correction (**k** in equation 1), implemented via a lookup table, is then applied in the **R** calculation to force the ratio at the center of each block to zero.

A given value of **R** is associated with an individual crystal within the block via a lookup table specifying the lower and upper levels of the ratio values for that crystal. A good event is recorded if the boundary conditions are met and the phototube-sum, or total energy, signal is within a window derived from the crystal energy spectra. Boundary and energy lookup tables are specified for each block to account for small variations in crystal properties and alignment. The determination of the lookup tables is an iterative process in which a starting set of boundaries are specified from **R** plots taken with wide energy windows, then a set of narrower energy windows are specified from the energy spectra and the process repeated until an optimum is reached.

Coincidence data are mapped to a sinogram format for storage, corrected for sensitivity, randoms and attenuation and reconstructed using a standard convolution-backprojection algorithm.

III. SYSTEM PERFORMANCE

Reconstructed resolution was measured using 0.42 mm diameter ^{18}F line sources (22 gauge needles). Reconstructions were done with a ramp filter having a cutoff frequency of 2 mm^{-1}. Figure 7 shows an example of these measurements and table 1 summarizes the results. The resolution at the center of the field is 1.25 mm and the radial resolution at 2.5 cm radius is 1.75 mm.
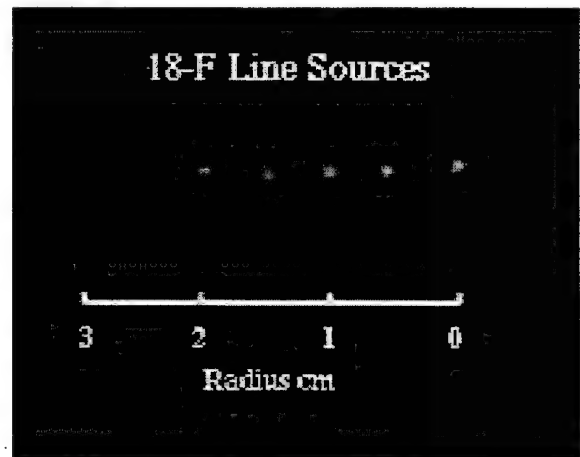

18-F Line Sources

Figure 7: Reconstructed Image of six 0.4mm 18F line sources 0.5 cm apart. The scale shown is at 1 cm intervals with the field center at the right.

developed. A multiple ring version of this instrument with somewhat larger detector-ring diameter is currently being designed.

V. ACKNOWLEDGMENT

VI. REFERENCES

[1] Del Guerra A, Scandola M and Zavattini G, "YAP-PET: First Results of Small Animal Positron Emission Tomograph Based on YAP:CE Finger Crystals." *IEEE Transactions on Nocl. Sci.*, 45:3105-3108, 1998.

[2] Pichler B, Boning G, Lorenz E, et. al., "Studies with a Prototype High Resolution PET Scanner Based on LSO-APD Modules", *IEEE Transactions on Nucl. Sci.* 45: 1298-1302, 1998.

[3] Cherry SR, Shao Y, Silverman RW, et. al. , "Micropet: a high resolution PET Scanner for Imaging Small Animals, *IEEE Transactions on Nucl. Sci.*, 44:1161-1166, 1997.

[4] Weber S, Terstegge A, Engels R, et al, The KFA TierPET: Performance characteristics and measurements." *IEEE Nuclear Science Symposium & Medical Imaging Conference Record*, 1117-1120, 1997.

[5] Watanabe M, Okada H, Shimaza K, et. al., A high resolution animal PET scanner using compact PS-PMT detectors, *IEEE Transactions on Nucl. Sci.* 44: 1277-1282, 1997.

[6] Bruynodonckx P,Xuan 1, Tavernier S, Zhang S, "Performerance of a small animal PET scanner based on photosensitive wire chambers, "*IEEE Nuclear Science Symposium & Medical Imaging Conference Record*, 11335-1340, 1997.

[7] Moses WW, Virador SE, Derenzo SE, et al, "Design of a High-Resolution, High-Sensitivity PET Camera for Human Brains and Small Animals." *IEEE Transactions on Nucl. Sci.*, 44:1487-1491, 1997.

[8] Lecompte R, Cardorette J, Rodrique S, et. al."Initial Results from the Sherbrooke Avalanche Photodiode Positron tomograph", *IEEE Transactions on Nucl. Sci.* 43:1952-1957, 1996.

[9] Bloomfield PM, Rajeswaran S, Spinks T,et. al., "The design and Physical Characteristics of a Small-Animal Positron Emission Tomograph", *Physics in Med. and Biol.*, 40:1105-1196, 1995.

[10] Seidel J, Gandler WR, Green MV, "A Very High Resolution Single Slice Small Animal PET Scanner Based on direct Detection of Coincidence Line Endpoints", *Journal of Nucl. Med.* 35:p 40P, 1994.

[11] Tavernier S, Bruyndonckx P and Zhang S, "A fully 3D small PET scanner.", *Phys. Med. Biol.*, 37: 635-643, 1992.

[12] Correia JA, Burnham CA , Kaufman D, et. al, "Small Animal PET imaging Device - Preliminary Design Study", *J. Nucl. Med.* 38:44P, 1997

[13] Burnham CA., Elliott JT., Kaufman D., Chesler DA., Correia JA and Brownell G.L, "Single Interaction PET Detectors.' *IEEE Transactions on Nucl Sci,* 37:832-835, 1990.

[14] Burnham C A, Kaufman D E, Chesler D A, Stearns C W, Correia J A, Brownell G L: "A low-Z PET detector", *IEEE Transactions on Nucl Sci* . 37:832-834, 1990.

[15] Melcher C.L. and Schweitzer J.S, "Cerium doped lutetium oxyorthosilicate: A fast, efficient new scintillator." *IEEE Transactions on Nucl. Sci.* , 39:502-505, 1992.

[16] Wong WH, Uribe J, Hicks K, et al, "A 2-dimensional detector decoding study om BGO arrays with quadrant sharing photomultipliers." *IEEE Transactions on Nucl. Sci.* NS41: 1453-1457, 1994.

No. 1257

FULL FOV HOLE ANGULATION ERROR MAPPING OF PARALLEL HOLE COLLIMATORS USING A PRETILTED COLLIMATED FLOOD SOURCE.

A. J. Arends, M.J. A. de Voigt, A. van Lingen*, Medical Physics Department, Catharina Regional Hospital, Eindhoven, The Netherlands; Eindhoven University of Technology, Accelerator Laboratory, Eindhoven, The Netherlands; Department of Nuclear Medicine, Free University Hospital, Amsterdam, The Netherlands. (100351)

Objectives: Hole angulation errors (HAE) lead to misregistration of events. For SPECT limits as low as 0.25° have been proposed. QC-methods using point sources yield only local HAE-values, while mapping methods published require dedicated hardware/software. We propose a simple method for full FOV HAE mapping, requiring only standard NM-equipment. **Method**: For low energy photons collimators show almost purely geometric transmission (Tr). The concept used is the strong dependence of geometric Tr through a stack of two collimators on their alignment. The collimator to be tested (A) is mounted on the detector, and placed closely above a *collimated flood source* (parallel reference collimator B, preferably Hi-Res, on top of a ^{57}Co or ^{99m}Tc flood source). *Pretilting* maximizes sensitivity (dTr/dα)for small HAE-values and yields directional information. We apply a pretilt angle β that leaves Tr(β) at ≈50% of Tr(0°). Two high count transmission scans are performed at orthogonal pretilts. Areas with HAE will show up as cold or hot zones, depending on their magnitude and direction relative to the pretilt applied. If B is clinically used too, positive findings require an additional test (rotate B or use a point source) to decide whether A or B contains HAE. **Results**: Sensitivity and lower detection limit of the method depend on: type of collimators A and B, counts acquired, and uniformity of detector and flood source. Using two LEHR's (hexagon 1.5x38mm and 1.4x32.8mm) we found a dTr/dα of **20%** per **0.25°** of HAE at β=1.9°. Four out of ten collimators showed unacceptable HAE during acceptance tests, and one at regular QC. **Conclusions**: The method proved to be valuable in acceptance tests and regular QC. It is sensitive and produces full FOV maps of HAE. Errors ≥0.25° are detectable and were observed in several collimators.

No. 1258

DEVELOPMENT OF A SMALL ANIMAL PET IMAGING DEVICE WITH RESOLUTION APPROACHING 1MM.

J. A. Correia*, C. A. Burnham, D. Kaufman, A. J. Fischman, Massachusetts General Hospital, Boston, MA. (500477)

Small animal imaging presents a situation where positron range effects and sampling are the dominant physical limitations to spatial resolution. Annihilation-pair non-colinearity and scatter are minimized due to the small dimensions of both instrument and subject. Theoretical and simulation studies support the idea that spatial resolution on the order of 1mm can be achieved with ^{18}F and ^{11}C. The availability of LSO as a scintillator material for PET makes possible the design of detector modules with resolution approaching one millimeter. The purpose of the work reported here was to design and construct a prototype single-plane, high resolution PET instrument using LSO detectors. The approach taken was to develop a simple prototype that maximizes the use of software data processing to minimize electronics construction. The detector array consists of a single ring of 360 1x4.5x5 mm LSO crystals organized into blocks of 12 crystals each viewed by two photomultipliers. To achieve high resolution, thin crystals (5 mm) are used for several reasons; first, the use of thin crystals moderates the degradation and non-uniformity of resolution caused by multiple detector penetration at photon incidence angles far from the normal, and secondly, blurring due to multiple interaction sites is reduced. The choice of thin crystals represents a sacrifice in sensitivity to preserve resolution. The system is also operated with a low energy threshold to maximize the number of single-interaction-site events. Crystals are identified using two block-specific lookup tables, one applied to the normalized pm tube differences and one applied to the total block energy. Reconstructed resolution was measured using 0.42 mm diameter 18F line sources. The resolution at the center of the field is 1.2 mm and the radial resolution at 2.5 cm radius is 1.65 mm. System sensitivity was measured using cylindrical water-bath sources of various diameters yielding 1.2 cps/uCi/cc for a 0.5 cm source and 72 cps/uCi/cc for a 4.5 cm source. Imaging studies in rats and mice with ^{18}F- FDG and several ^{11}C receptor compounds have been begun.

No. 1259

THE EVALUATION AND CALIBRATION OF FAN-BEAM COLLIMATORS.

J. L. Mahowald, P. D. Robins, M. K. O'Connor*, Mayo Clinic, Rochester, MN. (100046)

The aims of this study were a) to determine the true focal-length of a fan-beam collimator and b) to calibrate image size (mm/pixel) for each collimator to permit inter-comparison of image data acquired on different gamma camera systems. Methods: 6 fan-beam collimators were evaluated on 3 SPECT systems. Tomographic images of a line of Co-57 markers were obtained at 3 radii of rotation. From the transaxial images the distance between markers was measured in pixels and used to determine pixel size in mm / pixel. The system value for the focal length of the collimator was modified by up to + 100 mm and transaxial images were again reconstructed. SPECT images of a 3-D brain phantom were reconstructed using both the original and modified values of collimator focal length and thickness. Co-registration and subtraction of the reconstructed transaxial images was used to evaluate the effects of changes in collimator parameters. Results: Pixel size in the reconstructed image was found to be a function of both the radius of rotation and the focal length. At the correct focal length, pixel size was essentially independent of the radius of rotation. For all 6 collimators, true focal length differed from the original focal length by up to 26 mm. These differences in focal length resulted in up to 6% variation in pixel size between systems. Pixel size between the 3 systems was standardized by altering the value for collimator thickness. Subtraction of the co-registered SPECT images of the 3-D brain phantom was significantly improved after optimization of collimator parameters, with a 35-50% reduction in the standard deviation of residual counts in the subtraction images. Conclusion: Accurate knowledge of the focal length of a fan-beam collimator is an important parameter on multi-detector systems for optimum image quality and where accurate image co-registration is required.

No. 1260

EFFECT AND CORRECTION OF DETECTOR SAG IN SPECT SYSTEMS.

J. Peter*, D. R. Gilland, J. E. Bowsher, M. P. Tornai, R. J. Jaszczak, Duke University Medical Center, Durham, NC. (101118)

Objective: Large field-of-view SPECT detectors mounted to one side of the gantry ring may deflect, or sag, due to gravity. The goal of this study was to investigate the effect of detector sag on SPECT image quality. *Methods*: Monte Carlo simulations were performed for several SPECT geometries over a range of displacement magnitudes using analytical point source phantoms. Phantom data were reconstructed using FBP and OSEM. A fixed detector mounting point is located at the center of the gantry-side detector surface. As the detector rotates over 2π, angular displacement of the collimator plane is rotational about the mounting point in azimuthal direction, θ, in the collimator plane and in polar direction, ϕ, out of the collimator plane. The magnitude of displacement varies with projection angle α whereby $\theta(\alpha)$ and $\phi(\alpha)$ follow the same functional relationship but are shifted by $\pi/2$, i.e. extremal azimuthal displacement corresponds to zero polar displacement and visa versa. *Results*: The detector rotational displacement results in a non-uniform displacement map of points on the collimator surface; points further away from the mounting point have a longer displacement vector. Angular displacement artifacts are clearly identifiable in projection data sinograms: azimuthal detector sag leads to out-of-plane artifacts; polar displacement results in center-of-rotation artifacts. For a parallel beam detector with radius 40cm and maximum angular detector sag of 1.5deg, 1cm displacement artifacts and substantial shape distortions in the reconstructed image are visible. *Conclusion*: Slight detector sagging can introduce significant image artifacts. These results indicate the importance of minimizing sag when designing scanners. Also, detector sag could be modeled within iterative reconstruction algorithms, which can account for physical detector characteristics.

Performance of Small Animal PET Instrument with 1mm Resolution

J.A. Correia, C.A. Burnham, D.E. Kaufman and A.J. Fischman

Massachusetts General Hospital, and Harvard Medical School, Boston, MA

Abstract

A single-plane PET imaging instrument using LSO detectors has been constructed to demonstrate the feasibility of imaging at 1 mm spatial resolution. The performance of this instrument has been evaluated in phantoms and small animals. Measurements presented include spatial resolution, sensitivity, countrate performance, linearity and field uniformity. Examples of several mouse imaging studies are also presented.

I. INTRODUCTION

The purpose of the work reported here was to evaluate the performance of a single-plane prototype small-animal PET instrument developed at our laboratory. The rationale for developing this prototype was to demonstrate the feasibility of imaging small-scale objects, particularly mice, at 1 mm spatial resolution and further to gain knowledge which will be applied to a second-generation design. The evaluation presented here consisted of measurements of a number of the instrument's physical properties as well as applications to physiological imaging in mice.

II. SYSTEM DESCRIPTION

The PET imaging system has been described in detail elsewhere [1-2] and therefore, only a brief description will be given here.

The detector array consists of a single ring of 360 1 x 4.5 x 5mm LSO crystals [3] organized into 30 blocks of 12, each block being viewed by two photomultipliers (PMT's) in a one-dimensional implementation of the geometry proposed by Wong [4]. The detector-element size limits the spatial resolution. A detector radial dimension of 5mm was chosen to moderate the degradation and non-uniformity of resolution caused by multiple detector penetration at photon incidence angles far from the normal, and to reduce blurring due to multiple interaction sites [5]. This choice represents a sacrifice in sensitivity to preserve resolution.

The crystal interfaces within each block have different treatments to optimize the amount of light reaching the two phototubes. Typically, the light collected at the block center is approximately 1/3 that at the block edge. Outputs of the thirty PM tubes are processed for timing and amplitude signals. The average crystal energy resolution is 17%at the block center for 0.511 MeV photons.

The coincidence logic uses the timing signal to identify coincidence events from the central volume of the detector with a resolving time of 16ns. Identification of a coincidence event results in the simultaneous sampling and digitization of all the linear PMT signals and their transfer to a PC for processing.

The software identifies a block when the sum of adjacent PMT signals is greater than its neighbors. The normalized difference (ratio) of PMT signals in each identified block is determined. If energy criteria are met, a particular crystal is identified, otherwise the event is rejected. Ratio-boundary and energy lookup tables are specified for each block to account for small variations in crystal properties. Coincidence data are mapped to a sinogram format for storage and subsequently corrected for sensitivity, randoms and attenuation and reconstructed using a standard convolution-back-projection algorithm.
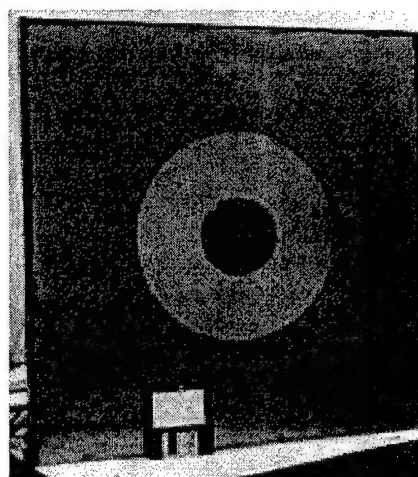

Figure 1: Photograph of PET Imaging System. A 3.5" computer disk is shown for scale.

III. SYSTEM PERFORMANCE

A number of physical performance measurements have been carried out in order to characterize the instrument's performance. These include both physical studies and preliminary imaging studies in mice. Summaries and specific examples are given in figures 2-11 and the text below. Studies were performed using a large-bore annular Pb collimator having an inside diameter of 7.5cm and a slice gap of 4mm.

The system in-plane spatial resolution was measured using 0.45 mm diameter line sources of ^{18}F placed at various distances form the center of the imaging field. The sources were filled with low levels of radioactivity to minimize countrates and therefore random coincidences. Images were reconstructed by filtered back-projection using a ramp filter. FWHM and FWTM were measured from profile plots through the reconstructed sources. These measured resolutions were corrected for finite source size by deconvolving the source response function. The results are shown in figure 2a. The resolution at the center of the field is 1.17mm and is 1.66mm at 2.5cm radius. An alternative measurement of the resolution is shown in figure 2b. 1cm x 1cm x 0.75cm-thick polyethylene blocks, each having an array of wells of varying size and spacing, were filled with ^{18}F solution and imaged. The smallest array, 1.25mm holes at 2.5mm separation is clearly visualized.

The axial resolution at the center of the field was measured by moving a point source of ^{18}F through the field in 0.1mm steps. The result was 1.75mm FWHM and 3.3mm FWTM as indicated in figure 3.

Figure 2b: Spatial resolution phantom consisting of 1 x 1 x 0.75cm polyethylene blocks containing arrays of ^{18}F-filled wells. The well diameters and spacings are indicated.

Figure 3: Axial response at field center measured by scanning a point source of ^{18}F in 0.1 mm steps. The FWHM = 1.75mm and the FWTM = 3.3m for the collimator gap used in the work presented here.

The system sensitivity was measured using 18F-filled cylinders of diameters from 0.5 to 4.5cm and a point source at the center of the field. The results for the cylinders are presented in figure 4 along with Montecarlo simulation results (solid line) for comparison. The point source sensitivity was measured to be 30 cps/uCi.
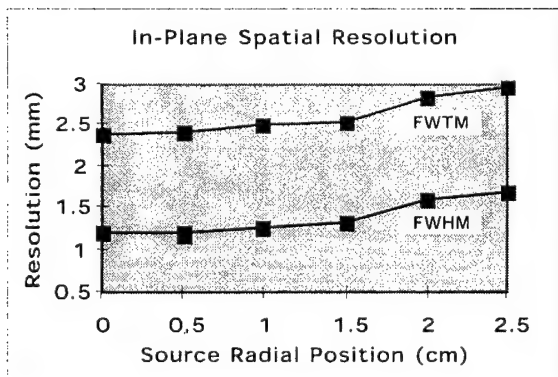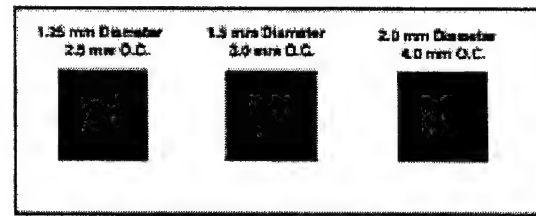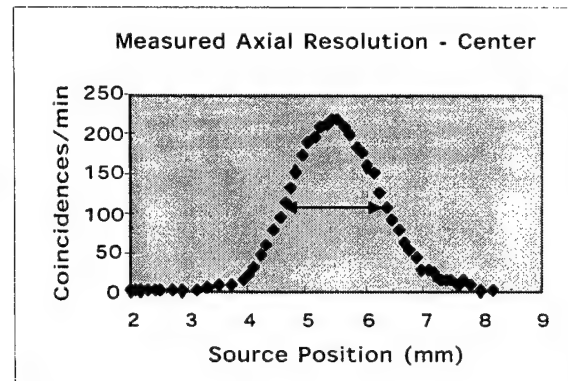

Figure 2a: Spatial resolution vs. field radius measured with 0.45 mm diameter line sources of ^{18}F. Corrected for finite source diameter. The FWHM and FWTM are shown.
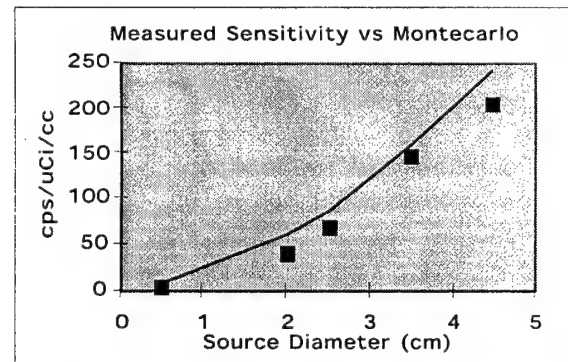

Figure 4: Measured sensitivity for cylindrical objects of varying diameter. The reported sensitivity includes all coincidence events above 150 keV. The solid line represents Montecarlo simulations of efficiency for 10 cm long cylinders under the same conditions.

The whole-field performance as a function of radioactivity concentration was measured using a 3cm diameter, 1cm long source of ^{13}N radioactivity. The measurements were made at the coincidence circuit output to eliminate the effects of the computer interface. The single channel events measured were the sum of all PMT timing signals and the coincidence rate measured includes all coincidences from within the central volume of the detector. The trues-data were corrected for randoms but not prompt scatter. Figure 5 shows the results of these measurements. The whole field rate at which randoms=trues is 60k trues/sec and little effect of deadtime was seen up to this rate. The singles/coincidence ratio was acceptably small over the whole range of the measurement.
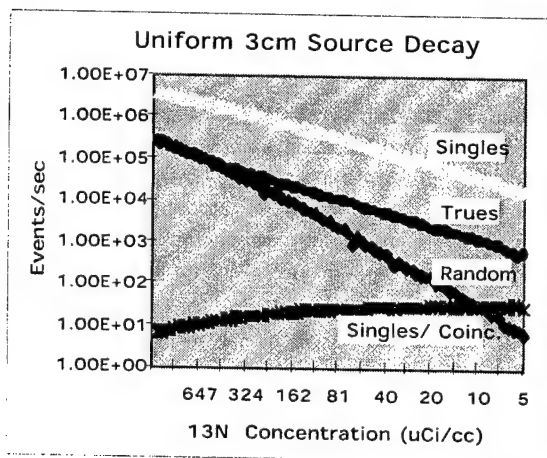

Figure 5: Measured whole field random coincidences, true coincidences, single events and single/coincidence ratio as a function of radioactivity concentration in a 3cm cylindrical object.
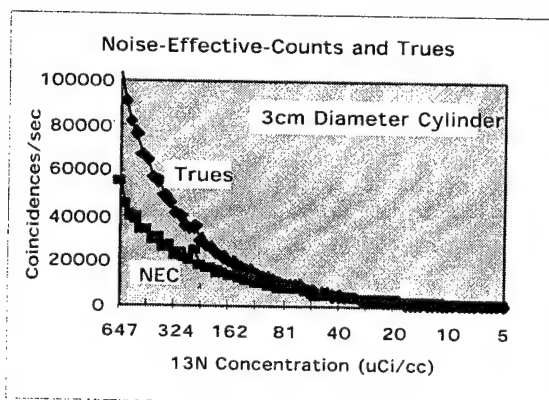

Figure 6: Noise equivalent count rate compared with true coincidence countrate up to randoms = trues for data presented in figure 5.

From these data the noise equivalent countrate as a function of radioactivity in the field was computed incorporating the scatter estimate discussed below. The results, compared to the true coincidence rate, are shown in figure 6.

The linearity of reconstructed activity concentration in small objects was measured over a range of 0.1 to 20 uCi/cc. Arrays of five 3mm diameter cylindrical sources placed at 1cm radius in a 3.5 cm absorber were imaged, reconstructed and relative concentration measurements extracted from ROI's placed over the sources. Figure 7 shows a plot of These results.. The solid line is a linear least squares fit to the measured points. The system is shown to be linear over the range of the measurements with r^2 =0.96. Also shown is a sample image from the measurement. The dynamic range of the concentrations in this image is approximately 5 to 1.
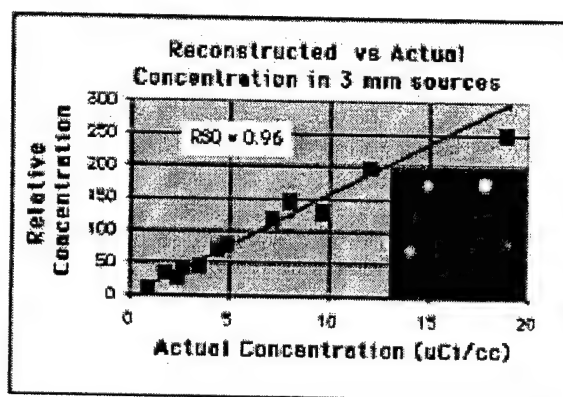

Figure 7: System linearity measured with arrays of five 3 mm diameter cylindrical sources located 1 cm from the field center. The sources were contained in a 3.5 cm diameter cylindrical absorber. The solid line is a linear least squares fit and the inset shows a sample image where the concentration dynamic range is 5 to 1.

The field uniformity of reconstructed data was measured in a 3.5cm-diameter uniform cylinder of ^{18}F radioactivity. 123 3mm circular ROI's were placed uniformly over the surface of the disk and relative-radioactivity-concentration values extracted. The variation in these values was found to be ± 5.4% (sample S.D.) and randomly distributed in an image with 3.5M coincidence events. The results are shown in figure 8.

These values are poorer than expected based on sampling considerations due in part to poor crystal identification at the block ends. This decreased resolution accounts for the fact that the measured resolution is fairly uniform over the central region of the field. The measured axial resolution of 1.75mm FWHM was obtained for the collimator used in the experiments presented here. By changing the collimator this resolution, as well as the inner diameter of the imaging aperture, may be varied; the range of slice thicknesses being limited on the low end only by system sensitivity and at the upper end by the 4.5mm crystal dimension. An alternative measurement of in-plane resolution, arrays of equi-spaced wells, indicates that high resolution (1.25mm) can be maintained in extended objects.

The system sensitivity for cylindrical objects and a point source at the center of the field agrees well with predictions from Montecarlo simulation although the measured sensitivities are systematically lower by about 20% in the cylinders and by 30% in the point source. The difference for the cylinders may be explained in part by the fact that poor light collection at the centers of the blocks gives rise to timing errors which result in the rejection of some good events. Both effects lead to underestimates of the sensitivity. In the case of the point source, small errors in source position may have a dramatic effect on the measured value and may account for the discrepancy.

The sensitivity is low due to two factors. The first is the use of detectors of limited radial dimension for the reasons stated above and the second is the need to limit events in a given crystal to a range of energies about the photopeak due to poor light collection from the center of the blocks. This process reduces the practical efficiency for useful events by 40-60% depending on the energy window-widths chosen.

The whole-system countrate measurements indicate that the system performs very well at high countrates showing little effect due to deadtime for activity concentrations up to about 800uCi/cc in a 2cm object. This is due in part to the fact that the data set generated is relatively small. The system is randoms limited and the point at which randoms=trues is 450uCi/cc (or alternatively 60,000 trues/sec). The robust behavior of the system in terms of randoms is explained by the highly restricted, single-plane, geometry.

Similarly, the scatter fraction measured with a line source at center-field surrounded by absorber yields a low result of 5.4% due to the restricted geometry. This result agrees fairly well with the 7.1% obtained from Montecarlo simulation.

Measurements of system linearity indicate that the system performs well over a range from 0.1-20 uCi/cc in small extended objects imbedded in absorber. Field uniformity in objects up to 3.5cm in diameter is about 5.4% (sample S.D.). This figure includes the effects of statistical fluctuations which, for the sizes or object and ROI's used in the measurements and the 3.5M events collected in the data set, is approximately 1.9% at the field center. The distribution of the fluctuations appears random.

The examples of mouse imaging studies shown demonstrate the resolution capabilities of the instrument as well as its limited sensitivity. The instrument may be effectively used for static imaging situations such as 18F-FDG imaging with moderate injected doses and may be useable, with larger injected doses, for some dynamic studies

The results of the studies presented here have led to several improvements which will be incorporated into a next generation device. These include: improved shielding design; improvements in block design particularly in terms of light output; redesign of the timing discriminator; and an improved PC interface.

V. ACKNOWLEDGMENTS

VI. REFERENCES

[1] Correia JA, Burnham CA , Kaufman D, et. al, "Small Animal PET imaging Device-Preliminary Design Study", *J. Nucl. Med.* 38:44P, 1997

[2] Correia JA, Burnham CA, Kaufman D, Fischman AJ, "Development of a Small Animal PET Imaging Device with Resolution Approaching 1 mm", *IEEE Transactions on Nucl.Sci.,* 46:631-635, 1999

[3] Melcher C.L. and Schweitzer J.S, "Cerium doped lutetium oxyorthosilicate: A fast, efficient new scintillator." *IEEE Transactions on Nucl. Sci.* , 39:502-505, 1992.

[4] Wong WH, Uribe J, Hicks K, et al, "A 2-dimensional detector decoding study on BGO arrays with quadrant sharing photomultipliers." *IEEE Transactions on Nucl. Sci.* NS41: 1453-1457, 1994

[5] Burnham CA., Elliott JT., Kaufman D., Chesler DA., Correia JA and Brownell G.L, "Single Interaction PET Detectors." *IEEE Transactions on Nucl Sci,* 37:832-835, 1990.

A PET Imaging Instrument for High Resolution Rat and Mouse Imaging

J.A. Correia, C.A. Burnham, D. Kaufman, E. Carter, A. Brownell and A.J. Fischman
Massachusetts General Hospital, and Harvard Medical School, Boston, MA 02114

The current frontier in PET instrumentation lies at devices which image at higher resolution over small-scale fields, with the goal of imaging small animals such as monkeys, rats and mice. Small animal imaging presents a situation where positron range effects and sampling are the dominant physical limitations. Annihilation-pair non-colinearity and photon scatter are minimized due to the small dimensions of both instrument and subject. The availability of LSO as a scintillator material for PET leads to several possible approaches to designing detector modules for PET systems having high spatial resolution. The purpose of the work reported here was to design, construct and apply a prototype PET instrument with resolution approaching 1mm using LSO detectors. The approach taken was to design and construct a simple single-plane instrument with as much flexibility as possible in hardware and software implementation. A simple design allows for straightforward modification and adaptation.

The detector array consists of a single ring of 360 1x4.5x5 mm LSO crystals organized into blocks of 12 crystals each viewed by two photomultipliers. Each phototube views two blocks. Thin crystals (0.5 cm) are used to moderate the degradation and non-uniformity of resolution caused by multiple detector penetration at photon incidence angles far from the normal, and minimize blurring due to multiple interaction sites. The choice of thin crystals represents a sacrifice in sensitivity to preserve resolution. The PM Tube signals are processed for timing and position. The coincidence logic uses the timing signal to identify any coincidence event from the central volume of the detector. The 30 linear position signals are DC coupled to the sample-and-hold ADC. Pulse shaping equivalent to a single delay line clipping is used. When a coincidence event is detected the 30 signals are simultaneously sampled and converted to thirty 8 bit words. The deadtime is limited by the time required to transfer, process and store an event in the PC. The preamplifiers, coincidence circuits and digital conversion circuits were implemented using standard logic elements.

The individual blocks were designed based a combination of computer simulations and experimental measurements of the optics for various geometries. The eight interior crystal faces are glued together in a jig with an 8o taper in order to point them toward the ring center. The next two on each side are separated from central crystals and each other by an air gap. The two outside crystals have polished surfaces and a partial reflector isolates them from the adjacent crystals. A reflector is used between blocks. Approximately 1/3 of the light from the peak signals is lost and the energy resolution of the blocks at 0.511 keV is 17%.

Individual crystals are identified using three look-up tables customized for each block. These tables determine if the value of the normalized phototube difference and the energy of the event fall within defined ranges. The third table specifies a normalization factor to adjust for phototube gain differences.

The in plane spatial resolution of the device has been measured to be 1.2 mm at the field center, 1.27 mm at 1 cm radius and and 1.55 mm at 2 cm radius using 0.4 mm diameter line sources of 18-F. The axial resolution is variable but has been operated to date at 1.8 mm. The point source sensitivity for a source at the field center has been measured to be 30 coincidences/sec/μCi using an 18-F point source.The instrument has been applied to the imaging of adult rat brain, juvenile rat torso and adult mouse brain and torso using 18F FDG and fluoride ion as well as several 11-C labeled neuro receptor compounds.

The possibility of PET imaging with LSO detectors at resolution approaching 1 mm has been demonstrated in a prototype single-plane instrument. Resolution degradation is moderated by the use of thin crystals to the degree that objects up to approximately 3.5 cm diameter show only minimal degradation and objects up to approximately 5 cm in diameter maintain off-center resolution below 2 mm. The sensitivity of the instrument is low due to the use of thin detectors to preserve resolution and the need to limit events in a given crystal to a range of energies about the photopeak due to poor light collection from the center of the blocks. This process reduces the efficiency for useful events by 30-60% depending on the energy window-widths chosen.

The most effective use of this instrument in the future is expected to be in imaging mice. Future plans include the characterization and refinement of the detector-block design, further characterization of crystal identification and time discriminator logic, corrections for other physical effects such attenuation, scatter and randoms in the projection data and design of a multiplane device.

HIGH RESOLUTION IMAGING IN SMALL ANIMALS WITH PET, MR AND OTHER MODALITIES

Instruments and Applications in Modern Biomedical Research

PROGRAM-ABSTRACTS

SEPTEMBER 27-29, 1999

ACADEMISCH ZIEKENHUIS VRIJE UNIVERSITEIT

AMSTERDAM, THE NETHERLANDS

[authors]
J. CORREIA, C. BURNHAM, D. KAUFMAN, A..FISCHMAN
Massachusetts General Hospital, Harvard Medical School

[title]
DESIGNS FOR SMALL ANIMAL PET INSTRUMENTS
[text]
We have recently constructed a single plane PET imaging instrument with 1.2 mm spatial resolution. It consists of a 12.4 cm ring of 360 1 x 4.5 x 5mm LSO crystals organized into blocks of 12. Thin crystals were used to minimize photon-multiple-scatter in the detectors. This choice was necessary to obtain high spatial resolution and minimize the effects of inter-detector penetration, but it resulted in a considerable loss of sensitivity. This instrument has been used to image mice and small rats. The 1 mm resolution design-goal was not reached due to difficulties in identifying the outer crystals in the blocks and poor timing and low sensitivity at the centers of some blocks.

A second generation device which acknowledges the above limitations has been designed and is under construction. This device uses 10 1.2 mm crystals per block, each crystal being increased from 5 to 7 mm in depth. The detector ring diameter has been increased to 15 cm. Increasing crystal depth and ring diameter result in a net increase in sensitivity of 1.85, improved crystal identification, and better timing response. Preliminary results indicate that the new blocks will function consistently at 1.2mm resolution. Several designs for multi-planar blocks are also being studied.

[keywords]
PET; Instrumentation; Detectors
[topic]
5 0 1
[programme]
SCI
[preference]
EITHER

Design Considerations for Small Animal PET Devices with mm Resolution.

J.A. Correia, C.A. Burnham, D. Kaufman, A.J. Fischman

Massachusetts General Hospital, and Harvard Medical School, Boston, MA 02114

Abstract

We have recently reported a single-plane LSO-based-PET instrument for imaging small animals. The thin detector employed 360 one mm LSO crystals. Images obtained were characterized by resolution approaching the sampling limit of 1mm.

Work directed at extending the performance of this instrument is reported here. A second-generation, single plane device is under construction and preliminary results for a multiplanar instrument have also been obtained.

I. INTRODUCTION

The purpose of the work reported here was to develop improved designs for the small-animal PET devices which are extensions of the 1 mm prototype PET described previously [1, 2]. This prototype consists of a single 12 cm diameter ring with 360 LSO detectors viewed by 30 photo-multiplier tubes (PMT's). A thin (5 mm) detector with a low energy threshold was used to maximize the detection of single-interaction events and minimize inter-element penetration for non-central lines of response.

Sensitivity is inherently limited by the low stopping power of the thin detector. It is further limited by the fact that the instrument images only a single plane. Although the expected transverse resolution of this system, dictated by sampling, was 1 mm, the actual resolution obtained at center field was approximately 1.2mm. Poor light collection at the center of the blocks resulted in poor timing and loss of low energy signals. Difficulty resolving crystals at the ends of the blocks limited resolution Despite these limitations applications to small animal imaging demonstrates the capabilities of high resolution imaging and the methodology developed to-date, as exemplified in figures 1 and 2.

Figure 1 shows selected transverse images of ^{18}F-FDG in the torso of a 25 gm mouse. Structures visible include the kidneys (leftmost image) and bowel (center image). Figure 2 shows a sequence of ^{18}F-fluoride-ion images of the leg of a 2.5 kg rabbit starting below the knee. The radius and ulna are clearly visualized and the periostial and endostial surfaces of the radius are fully separated.
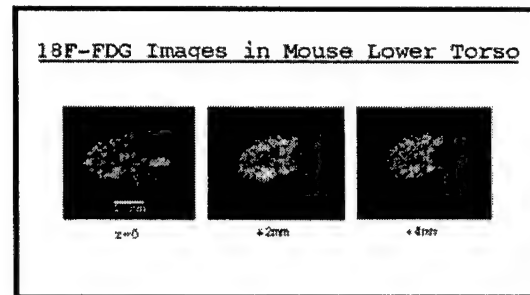

Figure 1: Sequential images of the lower torso in a 25 gm mouse begun 40 minutes after the injection of 2.4 mCi of 18F FDG. The plane separation is 2 mm. Each image was collected for approximately 15 minutes.
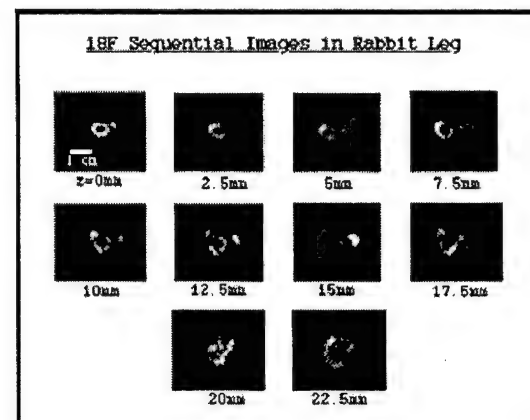

Figure 2: Sequential images, separated by 2.5 mm, of lower leg of a 2.5 kg rabbit begun twenty minutes after the injection of 15 mCi of 18-F Fluoride . The sequence moves up the leg toward the knee. Each image was collected for approximately 10 minutes.

A second generation, single-plane instrument has been designed and is under construction. The aim, as discussed below, was to improve sensitivity and overcome some of the performance limitations of the prototype.

Although a single-plane instrument is useful for some applications, it is limited by low sensitivity. We have therefore attempted to extend our present block-design to two dimensions. Such a detector element could form the basis of a future third-generation instrument with substantially higher sensitivity and multi-planar capability.

II. INSTRUMENT DESIGNS

The characteristics of the second and third generation instrument designs, compared to the completed prototype, are listed in table I. The second generation, single-plane instrument is currently under construction and is nearing completion. A detector for the third generation has been designed, a prototype block constructed and experimental evaluation begun. Both are discussed in more detail below.

A. Second Generation Single-Plane Instrument

The major changes from the prototype to the second-generation, single plane instrument are: (1) fewer crystal-elements per block to improve performance at 1.2mm resolution; (2) crystal elements of 7mm depth to improve stopping power and hence sensitivity and (3) a larger detector-array diameter of 14.7cm with a resulting increase of the number of PMT channels from 30 to 36. The results of imaging studies indicated that the 1mm resolution at the field center as dictated by sampling was not achieved in the prototype due to performance limitations of the 12-crystal detector-blocks. Further some loss of sensitivity was observed due to this limited performance. It was therefore decided to use slightly wider LSO crystals (1.2 mm) in the second generation design. This will limit the maximum resolution to the 1.2 mm achieved with the prototype but will improve the performance of the blocks considerably. Further, it was decided to increase the depth of the crystals from 5mm to 7 mm resulting in a factor of two improvement in sensitivity. Figure 3 shows a schematic diagram of the new detector block. The surface preparations shown in the diagram are similar to those of the 12-crystal block. The faces of the middle six crystals are glued together, the next one on either side is separated by an air gap and the outer two are separated by a translucent Teflon barrier.

Figure 4 shows the ratio spectrum measured from a uniform flux of 511 keV photons. The ratio is computed from the pmt signals as:

$$RATIO = (A - B)/(A + B).$$

	PROTO-TYPE	SECOND GENERATION	THIRD GENERATION
Diameter(cm)	12.3	14.7	14.7
LSO Crystals	360	360	360
Size (mm)	1x4.5x5	1.2x4.5x7	1.2x15x7
# PMT's	30	36	72
Resolution (mm)-Center	1.16	1.2	1.2
Resolution (mm)-2.5 cm	1.6	1.7	1.7
Sensitivity (cps/uCi)	35	>70	>500

Table 1: Properties of prototype, first generation and second generation PET instruments

The end crystals are more clearly resolved than those in the 12-crystal prototype block. Also, the range of pulse amplitudes between the center and edge crystals is lower than the corresponding range in the twelve-crystal block indicating better light collection at the block center. It is expected based on these improvements, that the uniformity of low-energy response will be improved resulting in an additional sensitivity improvement.
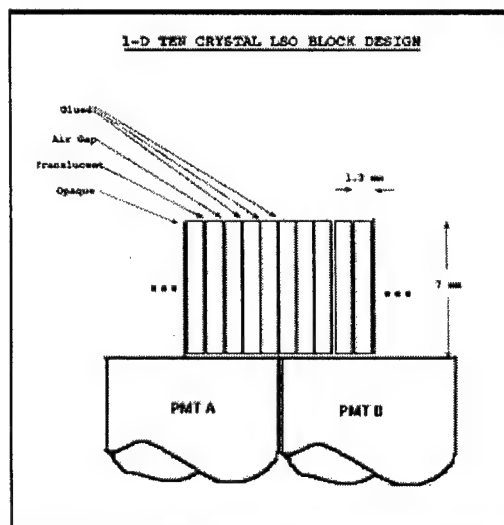

Figure 3: Sketch of 1-dimensional block consisting of ten 1.2x4.5x7mm LSO crystals. The surface treatments of the crystals are indicated.
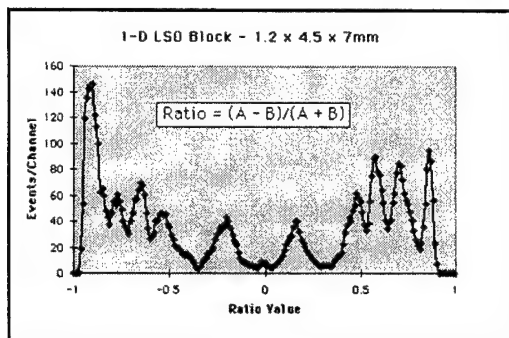
Figure 4: Measured ratio Spectrum for ten-crystal 1D block. The end crystals are more clearly resolved than those in the 12-crystal block. Also, the range of signal amplitudes between the center and edge crystals is lower than the corresponding range in the twelve-crystal block indicating improved light collection at the block center.

The front-end signal processing for the second generation instrument is similar to that of the prototype. When a coincidence event is detected by the electronics, all 36 PMT signals are systematically sampled, digitized and transferred to the computer where individual crystals are identified using four block-specific lookup tables; one each for ratio bounds, energy bounds, PMT-gain-correction and offset. A separate channel is used to collect the total detector singles rate. Thus the majority of processing is done in the computer allowing for a simple, flexible crystal identification procedure.
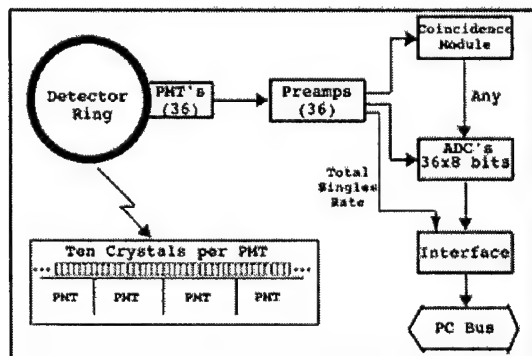

Figure 5: Schematic diagram of front-end processing electronics for second-generation instrument.

The photographs of Figure 6 show progress to date in the assembly of the second generation , single-plane instrument.
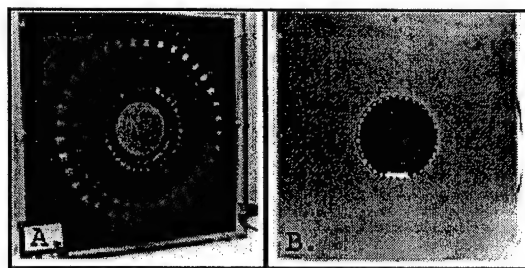

Figure 6: Photographs of the front and rear of the second generation instrument under construction. Left image shows PMT array and right shows the first few LSO blocks in place.

B. Third Generation 2D Detector Block Design

Although a single-plane instrument is capable of producing high-quality image data, its use is limited by sensitivity. In order to overcome this limitation, we have begun the development of a 2D-detector element with the eventual aim of designing a multiplanar instrument.

Most of the electronics and processing software developed for the single-plane designs was easily generalized for testing the 2D block. The single-plane block design was extended by increasing the crystal z-dimension from 4.5 to 15 mm and adding an additional row of PMT's as shown in figure 7. The basis of this design is that light collected and used to identify a given crystal within the block also contains information on the vertical (z) position of the interaction within the block. Thus, if the z thickness of the crystals is extended, it is possible not only to identify which crystal gave rise to the interaction but, by a separate computation using the same PMT signals, to obtain the z-coordinate of the interaction. The latter information can then be used to sort events into a set of transaxial planes, each one of which is equivalent to one data set collected by the single-plane instrument. Also, cross-plane coincidences can be used to further increase sensitivity.

The 2D-block was assembled with the same optical boundaries , shown in figure 3, as the 1D block. It was placed symmetrically on four PMT's as shown in figure 7. Measurements were made after adjusting the gains of the PMT's to give the same signal response to a uniform field.

A collimated line source of 511 keV photons, focused across the elements, was used to irradiate the block at several different z-positions with respect to the block-center. The radial ratio was calculated for a 10:1 range of whole-block signal response as follows:

$$RADIAL\ RATIO = [(A+C)-(B+D)]/[(A+C)+(B+D)].$$

21-43

Examples of these results are shown in figure 8 which gives the measured radial ratio at three different z-positions of the collimated source. All ten crystals are identified in each spectrum.

To assess axial performance, the z-axis ratio was measured for a 10:1 signal range using the same collimated line source. Measurements were made at the center, +/- 1.6mm and +/- 4.8mm and the z-axis ratios computed as follows:

$$Z\text{-}RATIO = [(A+B)-(C+D)]/[(A+B)+(C+D)].$$

Figure 9 shows the results of these measurements. The radial ratio at each source z-position was also calculated and each block-element was clearly identified. At distances greater than 5 mm from the block center the resolution is poorer but the z-ratio still maintains some sensitivity to change.
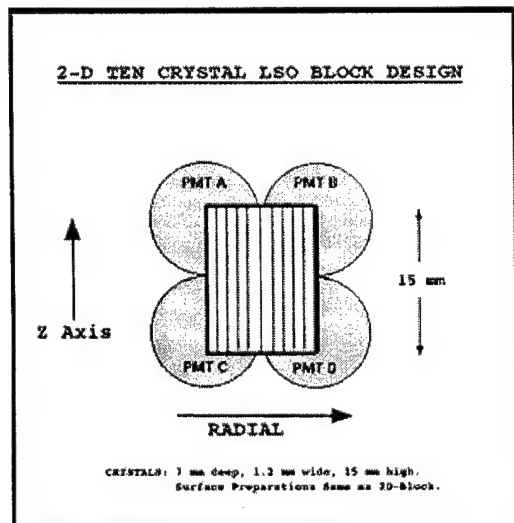

Figure 9: Axial ratio spectrum for a shielded line source of radioactivity placed at -4.8, -1.6, 0 +1.6 and + 4.8 mm with respect to the block center. The z-axis ratio is computed from the four PMT signals as indicated in the text.

Figure 7: Schematic of ten-crystal volumetric block. The z-dimension is the direction of the plane thickness in the single-ring instrument.
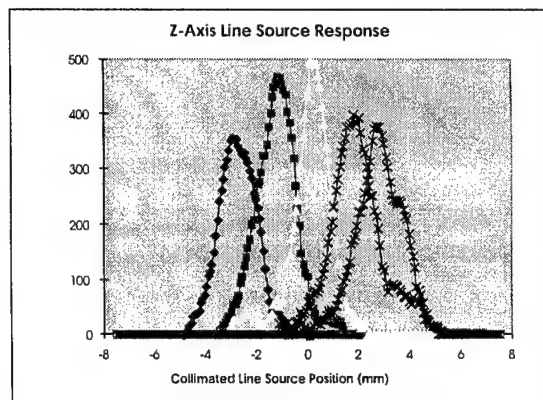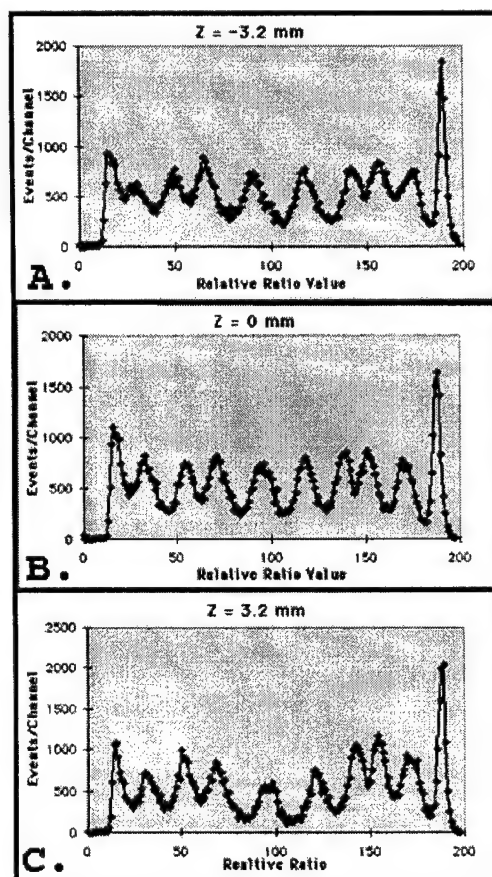

Figure 8: Examples of the 2D block radial ratio for different z-positions of a collimated line source computed from PMT signals as indicated in the text.

III. CONCLUSIONS

An improved single-plane small animal device has been designed and is under construction. Initial experiments with 10-crystal blocks indicate that crystal identification will be considerably improved compared to our prototype system. Further, improved timing stability, especially for events near the block centers, should result in increased and more uniform sensitivity. The use of etched, rather than polished crystals may lead to further improvement due to higher overall light output.

The detector ring diameter of the second generation instrument has been increased to 14.7 cm in order to offset the increased depth-of-interaction uncertainty due to the thicker detector. Further, the increase in diameter allows the instrument to accommodate larger objects such as a rat torso. The net increase in sensitivity resulting from the thicker detector and larger diameter is approximately a factor of two.

The third generation 2D-detector shows promise as an element for a multiplanar design. Although a uniform light background tended to compress the z-ratio spectra somewhat, the preliminary experimental results presented here indicate that at least 5 planes can be separated over the central 10 mm of the 15 mm detector. Over the same range the 10 crystals making up the block are well separated in the radial dimension.

A design based on a continuous detector in the z-dimension has several advantages. The first is ease of fabrication compared to two-dimensional arrays of individual detector elements. Secondly, the light losses are expected to be lower with the continuous z-detector element due to the higher volume-to-surface ratios of the detector elements. Finally, both the hardware and software developed for the single-plane devices is easily generalized and adapted to the continuous z design.

IV. ACKNOWLEDGMENTS

V. REFERENCES

[1] Correia JA, Burnham CA, Kaufman D, Fischman AJ, "Development of a Small Animal PET Imaging Device with Resolution Approaching 1 mm.", *IEEE Transactions on Nucl. Sci.* 45:631-635, 1999.

[2] Correia JA, Burnham CA, Kaufman D, Fischman AJ, "Performance of a Small Animal PET Instrument with 1 mm Resolution.", *IEEE Medical Imaging Conf, Conference Record.*, 1999.

HIGH RESOLUTION IMAGING IN SMALL ANIMALS:
Instrumentation, Applications and Animal Handling

PROGRAM-ABSTRACTS

SEPTEMBER 9–11, 2001
DoubleTree Hotel
Rockville, Maryland, USA

Design of a Volumetric High Resolution Small Animal PET

J.A. Correia, C.A. Burnham, D. Kaufman, and A.J. Fischman. Massachusetts General Hospital and Harvard Medical School, Boston.

Summary: We have recently developed two single-plane small animal PET imaging instruments which have spatial resolution of approximately 1 mm. These instruments employed 10 and 12 LSO detector elements respectively per photomultiplier tube. They have served mainly as demonstration prototypes for analog-coded LSO detector block designs but have also been used for numerous rat and mouse imaging studies. They are, however, limited by low sensitivity. By extending the axial length of the elements and adding a second ring of photomultiplier tubes, a high-resolution 2-dimensional block has been implemented. The detector consists of 1.2 mm wide × 7mm deep × 15mm high LSO crystals. The crystals are discrete in the radial dimension and continuous in the axial dimension. Event location in both dimensions is achieved using analog position sensing. A ten crystal block has been constructed and tested. Experiments with this detector block have demonstrated 1.2mm radial resolution and approximately 1.6mm axial resolution over the central 12mm of the 15mm detector element. A preliminary design for an instrument based on the 2-dimensional block has been generated. An instrument based on this design results in approximately a ten-fold increase in sensitivity compared to the single-plane designs.

Introduction: The purpose of the work reported here was to develop a design for a volumetric small animal PET instrument which is an extension of the prototype single-plane instruments described previously[1-3]. To-date a 2-dimensional block has been designed and experimentally evaluated, data acquisition and processing hardware have been redesigned for volumetric data acquisition, a preliminary data acquisition/processing algorithm has been designed and implemented and shielding design for the volumetric system has been undertaken. Both the data acquisition hardware and software are extensions of that previously reported for the single-plane systems.

Methods and Results: The surface preparation of the 2D-block is similar to that of the ten crystal 1-dimensional block. The faces of the middle six crystals are glued together, the next on either side is separated by an air gap and a Teflon film separates the outer two. Increasing the crystal axial dimension from 4.5 to 15 mm and adding an additional row of photomultipliers extended the single-plane block design. The basis of this design is that light collected and used to identify a given crystal within the block also contains information on the axial position of the interaction within the block. Thus it is possible not only to identify which crystal gave rise to the interaction but also, by a separate computation using the same photomultiplier signals, to obtain the axial coordinate of the interaction. In order to experimentally evaluate the axial resolution the block was placed symmetrically on four photomultipliers. Measurements were made after adjusting the gains of the photomultipliers to give the same signal response to a uniform field. A collimated line source of 511 keV photons, focused across the elements, was used to irradiate the block at several different axial positions with respect to the block-center. The radial ratio was calculated for a 5:1 range of whole-block signal response as follows:

$$\text{RADIAL RATIO} = [(A+C) - (B+D)]/[(A+C)+(B+D)].$$

Where A, B, C and D are the photomultiplier tube signals.

The z-axis ratio was measured for a 5:1 signal range using the same collimated line source. Measurements were made at the center, +/- 1.6mm and +/- 4.8mm and the axial ratios were computed as follows:

$$\text{AXIAL-RATIO} = [(A+B) - (C+D)]/[(A+B)+(C+D)].$$

The radial ratio at each source z-position was also calculated and each block-element was clearly identified. At distances greater than 5mm from the block center the resolution is poorer but the axial ratio still maintains some sensitivity to change.

The front-end signal processing for the 2D-instrument is similar to that of the single plane devices. Delay line like pulse shaping and leading edge timing are used to process the photomultiplier signals. When a coincidence event is detected, all 72 PMT signals are simultaneously sampled, digitized and then transferred to the computer where individual crystals and event axial position are identified using block-specific lookup tables; one each for ratio bounds, energy bounds, and PMT-gain-correction. Thus the majority of processing is done in the computer allowing for a simple, flexible crystal identification procedure.

The proposed 2D-instrument would consists of 360 LSO crystals organized into a 15cm diameter ring and viewed by two rings of 36 photomultipliers each. The expected spatial resolution, based of preliminary experimental measurements with prototype blocks will be 1.2mm radial at the field center, 1.7mm radial at 2.5cm radius and 1.6mm axial at the field center. The sensitivity will be approximately 500 cps/uCi.

Conclusions: The 2D-detector block shows promise as an element for a multiplanar design. Although a uniform light background tended to compress the axial ratio spectra somewhat, the experimental results presented here indicate that at least 5 planes can be separated along the 15mm detector. Over the same range, the 10 crystals making up the block are well separated in the radial dimension.

A design based on a continuous detector in the axial dimension has several advantages. The first is ease of fabrication compared to two-dimensional arrays of individual detector elements[4]. Secondly, the light losses are expected to be low, and thirdly, the axial length of the detector can be extended easily.

References:

[1] Correia JA, Burnham CA, Kaufman D, Fischman AJ, Performance of a Small Animal PET Imaging Device with 1mm Resolutionî, IEEE Trans. Nucl. Sci., IEEE Medical Imaging Conf, Conference Record. (1999).
[2] Correia JA, Burnham CA, Kaufman D, Fischman AJ, Development of a Small Animal PET Imaging Device with Resolution Approaching 1mm, IEEE Trans. Nucl. Sci. 46:631–635 (1999).
[3] Correia JA, Burnham CA, Kaufman D, Fischman AJ, Design Considerations for Small Animal PET Imaging î, IEEE Trans. Nucl. Sci., IEEE Medical Imaging Conf., Conference Record (2000).
[4] Burnham CA, Kaufman D, Chesler DA, Gregoire MC, Brownell GL MGH Cylindrical PET Operational Characteristics, IEEE Trans. Nucl. Sci. 2: 895–899 (1992).

simulations. **Results:** Using the proposed SBP scheme, an average spatial resolution of ~1 mm FWHM was obtained. The central field-of-view was 20×20 mm for SBP and 16×16mm for Anger decoding schemes respectively. **Conclusion:** A continuous detector module with intrinsic spatial resolution approaching 1 mm has been built and tested. Furthermore, the results demonstrate that our proposed positioning scheme yields improved performance over traditional Anger techniques for our proposed cMiCE detector.

No. 208

AN LSO-BASED DETECTOR ELEMENT FOR A MULTI-PLANAR SMALL-ANIMAL PET INSTRUMENT.

J. A. Correia*, C. A. Burnham, D. E. Kaufman, A. J. Fischman, Massachusetts General Hospital and Harvard Medical School, Boston, MA. (201200)

We have recently constructed two single-plane, small-scale PET instruments using LSO detectors. These instruments have demonstrated the feasibility of imaging at 1mm resolution in small objects but, while they are useful in many imaging situations, single-ring detectors are limited in sensitivity due to the small geometric solid angle subtended. To overcome this sensitivity limitation, we have generalized the detector block design used in the single-plane instruments by extending the axial dimension to form a multi-planar block. The design criteria were: (1) 1.2 mm spatial resolution at the field center; (2) simplicity and ease-of-fabrication of detector elements; (3) minimization of light losses in the small detector element. The multi-planar block design consists of ten LSO crystals, 1.2mm radial $\times$ 7mm thick $\times$ 15mm axial, attached at the 7×15mm faces. The central six crystals are glued together, the next one on ether side of center is separated by an air gap, and the outer one on either side by a partial reflector. The detector block is centered on an array of four PMT's. The PMT signals are used in several combinations to identify which crystal scintillated and where along the 15mm (z) dimension the scintillation took place. Preliminary experimental results indicate that, for 511 keV photons, the individual crystals can be clearly identified at z positions from 0 to $+/- 6$ mm re the detector-element center and that the z-dimension can be binned into at least 5 planes over the central 12 mm of the detector block. Light reflection at the crystal ends prevents identification of events for z $+/- 6$ mm in the current design. In addition to improving sensitivity, the block described here may provide opportunities for improved radial sampling, and hence, higher resolution. A multi-planar small-animal PET instrument based on this block is currently being designed. This work was supported in part by Department of Defense Grant #USAMRAA-DAMD17-98-8511.

No. 209

VALIDATION OF A NEWLY DEVELOPED PET CAMERA FOR SMALL LABORATORY ANIMALS BY MEANS OF *IN VIVO* AND *EX VIVO* NEURORECEPTOR IMAGING.

R. Larisch*, S. Nikolaus, M. Beu, K. Hamacher, H. H. Coenen, H. Vosberg, H. W. Muller-Gartner, Heinrich-Heine-University, Duesseldorf, Germany; Institut fuer Nuklearchemie, Forschungszentrum, Juelich, Germany. (201347)

Objectives: Recently, a high resolution 3D positron emission tomograph (TierPET) was developed for *in vivo* studies in small laboratory animals (axial and transaxial diameter of field of view: 40 mm; sensitivity: 3.24 cps/KBq with a center-detector-distance of 80 mm; resolution: FWHM 2.1 mm). In the present study, this system was validated for cerebral receptor imaging. **Methods:** The radiotracer concentrations were quantified *in vivo* with PET and immediately afterwards *ex vivo* with storage phosphor autoradiography. The correspondence between both methods was assessed by means of correlation analysis. In ten Sprague-Dawley rats, striatal radioactivity was measured after injection of 60 $\pm$ 10 MBq of the dopamine D_2 receptor ligand ^{18}FN-methyl-benperidol in six time frames of six minutes each. Upon completion of the scans, animals were sacrificed, their brains removed and cryosectioned (2.2 to – 2.3 mm from Bregma). Coronal slices were subjected to storage phosphor autoradiography. Striatal radioactivity was quantified in both modalities using region-of-interest analysis and activity standards. **Results:** After correction for decay, partial volume effect, and spill-over from the Harderian glands, the median of striatal radioactivity concentration was 0.38 MBq/ccm, (25. percentile: 0.3, 75. percentile: 0.43) measured with PET and 0.42 MBq/ccm (25. percentile: 0.24, 75. percentile: 0.51) measured with phosphor screen imaging. Correlation of striatal radioactivity

values yielded a Pearson correlation coefficient of 0.82 (p = 0.002). **Conclusion:** The results show a significant positive correlation between radioactivity values obtained with PET and storage phosphor autoradiography used as gold standard. Thus, the developed PET system is suitable for *in vivo* receptor binding studies in small laboratory animals.

Instrumentation & Data Analysis Track
Image Generation: Attenuation Correction Methods

2:30PM–4:00PM	Session 31	Room: 801 A

Moderator: Benjamin M. W. Tsui, PhD
Co-Moderator: Ronald H. Huesman, PhD

No. 210

DUAL-MODALITY PET/CT IMAGING: CT-BASED ATTENUATION CORRECTION IN THE PRESENCE OF CT CONTRAST AGENTS.

T. Beyer*, D. W. Townsend, CTI PET Systems Inc, Knoxville, TN; University of Pittsburgh Medical Center, Pittsburgh, PA. (200453)

Objectives: We have described previously [Kinahan et al., 1998] an algorithm for CT-based attenuation correction of dual-modality PET/CT emission data. This algorithm transforms the CT transmission images that are acquired as part of the PET/CT scan to attenuation maps at 511keV, that are used for attenuation correction of the emission data. This algorithm must be extended to account for the presence of CT contrast agents administered as part of standard radiological procedures. **Methods:** The attenuation maps at 511keV are calculated from the CT transmission images by a hybrid segmentation-scaling algorithm that is based on classifying CT image voxels as soft tissue and bone. In the current implementation, the effect of contrast is neglected. In CT images, contrast-enhanced tissues and structures can be distinguished from surrounding non-enhanced structures, whereas at 511 keV they have similar attenuation properties. The hybrid correction algorithm has been modified such that contrast-enhanced soft tissues are separated from non-enhanced tissues and bone in the original CT images. A third, independent scale factor is introduced for the transformation of attenuation values of contrast-enhanced tissues with attenuation values between 0HU and 300HU. The scale factors used are estimated from calibration procedures. **Results:** The CT-based attenuation correction algorithm has been successfully modified to account for the presence of CT contrast agents during the CT examination as part of a combined PET/CT imaging protocol. Data from phantom and whole-body patient scans are presented to illustrate the accuracy of the algorithm under clinical conditions. **Conclusion:** Using the modified hybrid algorithm, accurate attenuation correction of the emission data is possible without the requirement for either a standard PET transmission scan or a non-enhanced CT scan. Kinahan, PE, et al., Med Phys 25 (10): 2046pp, 1998.

No. 211

CT-BASED ATTENUATION CORRECTION: THE EFFECTS OF IMAGING WITH THE ARMS IN THE FIELD OF VIEW.

J. Carney*, D. W. Townsend, P. E. Kinahan, T. Beyer, M. Kachelriess, W. A. Kalender, B. De Man, J. Nuyts, University of Pittsburgh, Pittsburgh, PA; CTI PET Systems, Inc., Knoxville, TN; Institute of Medical Physics, University of Erlangen, Erlangen, Germany; University Hospitals Leuven, Leuven, Belgium. (201001)

Objectives: The standard practice in CT chest/abdominal imaging is to have the arms positioned above the head, outside the field of view. However, in combined PET/CT tomographs the arms will generally be in the field of view, since the longer PET acquisition time would lead to discomfort (and possibly more patient motion) otherwise. This leads to two problems in the resulting CT images: (1) Truncation artifacts appear if the arms extend outside the (CT) field of view. (2) Dark bands corresponding to lower attenuation values can appear between the arms. In order to ensure accurate attenuation values these effects (1, 2) must be corrected for prior to the CT-based attenuation correction being applied to the PET emission data. **Methods:** We reconstruct the CT image from the projection data over a larger field of view to include the arms, employing a sum rule that any integrated parallel projection should give the total integrated attenuation. Truncated projections (which give a lower total